



Published in final edited form as:

Dev Cell. 2019 May 20; 49(4): 542–555.e9. doi:10.1016/j.devcel.2019.03.003.

The long non-coding RNA *lep-5* promotes the juvenile-to-adult transition by destabilizing LIN-28

Karin C. Kiontke¹, R. Antonio Herrera^{1,2,6}, Edward Vuong^{3,7}, Jintao Luo³, Erich M. Schwarz⁴, David H. A. Fitch^{1,5,*}, Douglas S. Portman^{3,8,*}

¹Center for Developmental Genetics, Department of Biology, New York University, 100 Washington Square East, New York, NY 10003

²Department of Applied Mathematics and Statistics, Laufer Center for Physical and Quantitative Biology, Stony Brook University, Stony Brook, NY 11794-5252

³Departments of Biomedical Genetics and Neuroscience, University of Rochester School of Medicine and Dentistry, 601 Elmwood Avenue, Rochester, NY 14642

⁴Department of Molecular Biology and Genetics, Biotechnology 351, Cornell University, Ithaca, NY 14853-2703

⁵Arts & Sciences, New York University Shanghai, 1555 Century Ave., Pudong New Area, Shanghai, China 200122

⁶Current affiliation: Dyson College of Arts & Science, Pace University, New York, NY 10038

⁷Current affiliation: Department of Medicine, Long Island Jewish Medical Center, 270-05 76th Ave., New Hyde Park, NY 11040

⁸Lead Contact

SUMMARY

Biological roles for most long non-coding RNAs (lncRNAs) remain mysterious. Here, using forward genetics, we identify *lep-5*, a lncRNA acting in the *C. elegans* heterochronic (developmental timing) pathway. Loss of *lep-5* delays hypodermal maturation and male tail tip morphogenesis (TTM), hallmarks of the juvenile-to-adult transition. We find that *lep-5* is a ~600-nt cytoplasmic RNA that is conserved across *Caenorhabditis* and possesses three essential secondary structure motifs but no essential open reading frames. *lep-5* expression is temporally

* **Correspondence:** Douglas S. Portman, Ph.D., Department of Biomedical Genetics, University of Rochester School of Medicine and Dentistry, 601 Elmwood Avenue, Rochester, NY 14642, douglas.portman@rochester.edu, Phone: 585-275-7414; David H. A. Fitch, Ph.D., Department of Biology, New York University, 100 Washington Square East, New York, NY 10003, david.fitch@nyu.edu, Phone: 212-998-8254.

AUTHOR CONTRIBUTIONS

Conceptualization, K.K., D.S.P., R.A.H., E.M.S., E.V. and D.H.A.F.; Methodology, R.A.H., K.K., J.L., D.S.P., E.M.S. and E.V.; Investigation, R.A.H., K.K., J.L., D.S.P., E.M.S. and E.V.; Writing – Original Draft, K.K., E.V. and D.S.P.; Writing – Review & Editing, D.H.A.F, K.K., D.S.P. and E.M.S.; Funding Acquisition, D.H.A.F and D.S.P.; Supervision, D.H.A.F and D.S.P.

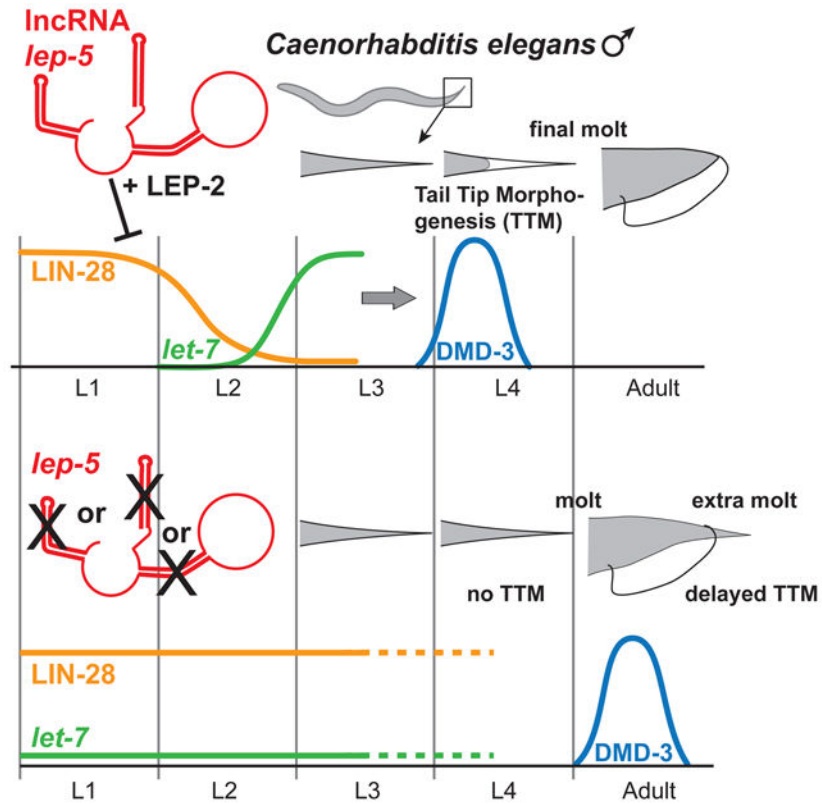
DECLARATION OF INTERESTS

The authors declare no competing interests.

Publisher's Disclaimer: This is a PDF file of an unedited manuscript that has been accepted for publication. As a service to our customers we are providing this early version of the manuscript. The manuscript will undergo copyediting, typesetting, and review of the resulting proof before it is published in its final citable form. Please note that during the production process errors may be discovered which could affect the content, and all legal disclaimers that apply to the journal pertain.

controlled, peaking prior to TTM onset. Like the Makorin LEP-2, *lep-5* facilitates the degradation of LIN-28, a conserved miRNA regulator specifying the juvenile state. Both LIN-28 and LEP-2 associate with *lep-5* *in vivo*, suggesting that *lep-5* directly regulates LIN-28 stability and may function as an RNA scaffold. These studies identify a key biological role for a lncRNA: by regulating protein stability, it provides a temporal cue to facilitate the juvenile-to-adult transition.

Graphical Abstract



eTOC BLURB

The functions of most long non-coding RNAs (lncRNAs) are unknown, despite their abundance in biological systems. Here, by characterizing *C. elegans* mutants with developmental delays, Kiontke *et al.* identify *lep-5*, a ~600-nt lncRNA. *lep-5* regulates developmental timing by binding to and destabilizing LIN-28, a conserved regulator of miRNA biogenesis.

Keywords

C. elegans; lncRNA; lincRNA; heterochronic; developmental timing; male tail; morphogenesis

INTRODUCTION

Long non-coding RNAs (lncRNAs), once thought to be biological noise, are now appreciated as important components of many biological processes. These 200nt long non-coding transcripts are associated with remarkably diverse molecular functions, including

regulation of chromatin topology and modification, transcriptional activation, control of miRNA availability, and scaffolding of proteins and RNAs. lncRNAs act in diverse developmental processes including pluripotency, patterning, and differentiation, and are also implicated in the pathogenesis of neurodegeneration and cancer (Cech and Steitz, 2014; Delas and Hannon, 2017; Fatica and Bozzoni, 2014; Geisler and Collier, 2013; Quinn and Chang, 2016; Ransohoff et al., 2018). While most lncRNAs function in the nucleus, some have cytoplasmic functions, *e.g.*, TINCR brings together Staufen and mRNAs that promote epidermal differentiation (Kretz et al., 2013) and HOTAIR scaffolds the E3 ubiquitin ligases Dzip3 and Mex3b with their respective substrates Ataxin-1 and Snurportin-1 to prevent premature senescence (Yoon et al., 2013). However, biological roles and molecular functions remain unknown for the vast majority of lncRNAs, particularly for those that act in the cytoplasm.

In the nematode *C. elegans*, numerous lncRNAs have been detected by high-throughput approaches, but relatively little is known about their functions or roles in biological processes (Liu et al., 2017b; Nam and Bartel, 2012; Wei et al., 2019). For another important family of ncRNAs, the microRNAs (miRNAs), essential insights came from forward genetic approaches. The first two known miRNAs in any system, *lin-4* and *let-7*, were identified in a series of classic studies on *C. elegans* developmental timing mutants (Ambros, 1989; Lee et al., 1993; Reinhart et al., 2000; Wightman et al., 1993). Both of these miRNAs function in the *C. elegans* heterochronic pathway, a mechanism that controls developmental progression through four larval stages into adulthood (Rougvie and Moss, 2013). In heterochronic mutants, certain stage-specific developmental events occur too early (“precocious” mutants) or too late (“retarded” or delayed mutants). Interestingly, regulation by non-coding RNAs figures prominently in the heterochronic pathway: in addition to *lin-4* and *let-7*, the *lin-4*-related *mir-237* and three other *let-7*-like miRNAs, *mir-48*, *-84* and *-241*, also have key roles (Abbott et al., 2005; Tsialikas et al., 2017). Expression of these miRNAs in successive temporal waves during larval development keeps the activities of their targets in check until the appropriate time (Ambros, 2011).

Several key components of the heterochronic pathway, most notably the miRNA *let-7* and its negative regulator LIN-28, are functionally conserved in animals (Faunes and Larrain, 2016). While *lin-28* orthologs promote an immature state associated with stemness and multipotentiality, *let-7* promotes differentiation and maturation. For example, *Drosophila let-7* regulates the timing of neuromuscular remodeling during metamorphosis (Caygill and Johnston, 2008; Sokol et al., 2008) and the temporal patterning of neural cell fates in the brain (Wu et al., 2012). In mammals, LIN28 promotes stem cell pluripotency (Copley et al., 2013; Zhang et al., 2016) and is genetically linked to the timing of the juvenile-to-adult transition (Faunes et al., 2017; Ong et al., 2009; Perry et al., 2009; Zhu et al., 2010).

The *lin-28-let-7* system also controls the juvenile-to-adult transition in *C. elegans* (Del Rio-Albrechtsen et al., 2006; Herrera et al., 2016; Rougvie and Moss, 2013; Vadla et al., 2012). A hallmark of this transition is male tail tip morphogenesis (TTM). TTM occurs during the fourth larval stage (L4) and involves the fusion and retraction of the four tail-tip hypodermal cells, hyp8-11, to generate the rounded tail tip characteristic of the adult male (Figs. 1A, B) (Nguyen et al., 1999). In retarded *lin-41(gf)*, *let-7(rf)* and *lep-2(lf)* mutants, TTM is delayed

or absent. This leads to the perseverance of a juvenile tail tip in adults, a phenotype called Lep (leptoderan). Conversely, TTM initiates early in *lin-41(lf)* and *lin-28(lf)* mutants, resulting in an over-retracted (Ore) phenotype in adults (Del Rio-Albrechtsen et al., 2006; Herrera et al., 2016; Vadla et al., 2012). The Lep and Ore phenotypes of these mutants result from alterations in the timing of the expression of *dmd-3*, a *doublesex-family* transcription factor that governs execution of the TTM program (Mason et al., 2008; Nelson et al., 2011). While the role of the heterochronic pathway has been intensively investigated in the division and differentiation of the lateral seam cells, little is known about this pathway in other cell types, or the extent to which it regulates other aspects of developmental timing. TTM provides an outstanding opportunity to address this gap.

Here, we report the identification and characterization of *lep-5*, mutations in which disrupt the onset of TTM as well as other aspects of the larval-to-adult transition. We find that *lep-5* expression is under temporal control and that it acts in the heterochronic pathway to promote the degradation of LIN-28. Surprisingly, *lep-5* acts as a lncRNA that is conserved across the *Caenorhabditis* genus. These findings highlight the role of lncRNAs as mediators of protein stability and emphasize the importance of ncRNAs in developmental timing.

RESULTS

lep-5 mutant males fail to undergo normal tail tip morphogenesis

Using a forward genetic approach, we identified two X-linked mutants, *ny10* and *fs8*, with defects in TTM. As adult males, both mutants exhibit long, pointed (Lep) tail tips that protrude far outside the cuticular fan (Fig. 1C, D). Other aspects of male tail anatomy appeared normal. In particular, the “anterior retraction” process, which generates the rays and fan and is mechanistically distinct from TTM (Nguyen et al., 1999; Sulston et al., 1980) was not disrupted in *lep-5* males (Figs. 1C, D). Complementation tests showed that *ny10* and *fs8* are recessive and allelic (see STAR Methods). We named the gene identified by these mutations *lep-5*. The Lep phenotype of *ny10* was completely penetrant at 15°C and 25°C, whereas that of *fs8* was temperature-sensitive (Table 1), suggesting that *fs8* is a hypomorphic allele.

Consistent with the Lep phenotype, we observed that tail tip cells in *lep-5* L4 males failed to undergo normal migration and retraction. Using the adherens junction marker AJM-1::GFP, we found that some hyp cells remained unfused even in adult *lep-5* males (Fig. 1G). Thus, *lep-5* influences both cell fusion and retraction, indicating that it regulates the execution of the entire TTM program (Nguyen et al., 1999).

In addition to TTM defects, we observed several mutant phenotypes that suggested a more general role for *lep-5* in developmental timing. In some *lep-5* males, delayed TTM occurred in adults (Fig. 1H). Furthermore, 42% of *lep-5* males (n = 101) and 62% of *lep-5* hermaphrodites (n = 101) molted again in adulthood, a characteristic of some other developmental timing mutants (Ambros and Horvitz, 1984) (Fig. 1I, Fig. S1). In males, these supernumerary molts were invariably lethal, while in hermaphrodites, they led to defects in vulva morphology (Fig. S1K). The adult alae, stage-specific specializations of the lateral hypodermis, appeared normal in males, but in hermaphrodites, alae were weak or

partially absent in most young adults (Fig. S1). Despite this, adult seam cell numbers ($n = 50$ sides) and seam cell fusion were normal in *lep-5* mutants of both sexes, and we found no evidence for additional seam cell divisions in adults. We conclude that *lep-5* function is important for some but not all somatic features of the juvenile-to-adult transition in *C. elegans*.

***lep-5* alleles identify a previously uncharacterized gene**

Using standard methods, we mapped *lep-5* to the uncharacterized predicted gene H36L18.2 (Fig. S2). Transcriptome sequencing indicates that H36L18.2 produces a mature polyadenylated RNA of ~600 nt after the removal of two introns and trans-splicing to the SL1 splice leader (Gerstein et al., 2010) (Fig. 2A). We found that *ny10* was a large, ~80-kb deletion encompassing 32 predicted genes (Fig. S2), while *fs8* was a point mutation (G23A) in the first nucleotide following the SL1 acceptor site (Fig. S2C). We also engineered a *lep-5* null allele, *ny28*, by CRISPR. While most experiments described below were carried out using *ny10* and *fs8*, we found that *lep-5(ny28)* null mutants phenocopied *lep-5(ny10)* with respect to all phenotypes described above (Table 1). Furthermore, the *lep-5(ny10)* phenotypes in males and hermaphrodites are rescued by a transgene covering a region from 3838 nt upstream to 248 nt downstream of the wild-type H36L18.2 locus ($n > 50$).

The mature H36L18.2 transcript has three potentially translatable regions, encoding conceptual products of 34 (ORF1), 83 (ORF2), and 106 (ORF3) amino acids. One of these (starting at M12 of ORF2) was identified as predicted ORF in the WormBase genome annotation WS250. None of the three possible translation products have detectable domains or homology to any other known proteins. Remarkably, however, the primary nucleotide sequence of *lep-5* was strongly conserved in the genomes of 18 other *Caenorhabditis* species in the *Elegans* group (Kiontke et al., 2011) and less well conserved in seven more distantly related species (Fig. S3). While most of these *lep-5* orthologs contain potentially translatable regions, there is no detectable similarity in their potential protein products or in their positions in the predicted transcripts (Fig. S4).

These findings raised the possibility that *lep-5* function depends on nucleotide sequence itself rather than coding potential. As an initial test of this idea, we asked if expression of *lep-5* orthologs from *C. briggsae* (*Cbr-lep-5*) or the more highly divergent *C. angaria* (*Can-lep-5*) could rescue the tail-tip defects of *C. elegans lep-5* (*Cel-lep-5*) mutants. *Cbr-lep-5* and *Can-lep-5* each have one potential ORF, but these share no coding potential with each other or with the potential ORFs in *Cel-lep-5*. Remarkably, we found that expression of *Cbr-lep-5* completely rescued and *Can-lep-5* partially rescued the Lep defect of *C. elegans lep-5* mutants (Fig. 2C). These results very strongly suggest that the putative ORFs of *lep-5* are not required for its function. Note that polyadenylation, as observed in *lep-5*, is a feature of many non-coding transcripts (Kopp and Mendell, 2018; Nam and Bartel, 2012).

***lep-5* is a lncRNA with several prominent secondary structure motifs**

To predict *lep-5* secondary structure, we used TurboFold (Harmanici et al., 2011) for comparative analysis of *lep-5* orthologs from 19 species in the *Elegans* group of *Caenorhabditis*. This revealed several notable features (Figs. 2A, S4, S5). First, *lep-5* RNA is

predicted to be highly structured, with multiple stem-loops, several prominent single-stranded regions, and a central “zipper” region. Most of the base-paired regions show high conservation; many predicted single-stranded positions are also strongly conserved, suggesting that these might serve as sites for interactions in *trans* (Fig. 2A). Second, the extensive base-pairing, particularly in the central zipper region, suggests that the mature RNA adopts a compact structure. Third, the very 5′ end of the *lep-5* RNA is predicted to fold into a 53-nt stem-loop structure that includes the 22-nt trans-spliced leader SL1. A consensus structure derived from alignment of the 21 *Elegans*-group *lep-5* genes, as well as individual TurboFold-predicted structures, indicated that three key features are conserved in all orthologs: the 5′ SL1-containing stem-loop, the central zipper region, and a stem-loop near the 3′ end (Fig. 2A, Fig. S4).

Interestingly, the position altered in the *lep-5(fs8)* mutant (G23A) lies near the tip of the 5′ stem-loop and is predicted to base-pair with C30. This mutation dramatically altered the predicted structure of the 5′ region, replacing the large stem-loop with several smaller double-stranded regions (Fig. 2B, S3B). To ask whether base-pairing between positions 23 and 30 is important for *lep-5* function, we created rescue constructs containing the G23A mutation alone and in combination with a second mutation, C30T, a compensatory change predicted to restore the 5′ stem-loop (Fig. 2B). While the G23A mutant transgene had poor rescue activity, the G23A C30T double mutant transgene completely rescued the *lep-5* tail tip phenotype (Fig. 2C). Introducing a different mutation at this position, G23C, alone and together with its corresponding compensatory change, C30G, yielded the same pattern of results (Fig. 2C). These experiments indicate that base-pairing between G23 and C30 is critical for *lep-5* function, strongly supporting the existence of the 5′ stem-loop *in vivo*.

To probe additional regions that could be important for *lep-5* function, we deleted two predicted internal stem-loops from the rescue construct. “ 1” (482-G542) removes most of the large, well-conserved predicted stem-loop near the 3′ end of *lep-5* (Fig. 2A). This deletion abolished rescue activity (Fig. 2C). Deletion of a less well-conserved smaller internal stem-loop (“ 2”, T216-A257) reduced, but did not eliminate, rescue (Figs. 2B, C). In contrast, introducing multiple stop codons into the putative ORF2, at codons 15, 16, and 17 (“*3 stops”) or at codons 25 and 26 (“*2 stops”), did not diminish the ability of these constructs to rescue *lep-5* (Figs. 2C,D).

To further explore the structure of the *lep-5* lncRNA and to confirm the dispensability of its putative ORFs for *lep-5* function, we created several new *lep-5* CRISPR alleles (Fig. 2D). *lep-5(fs18)* is a TT193AAA change that introduces a stop codon and frameshift into ORF2 but is not expected to significantly alter RNA secondary structure. These mutants were phenotypically wild-type (Figs. 2D, E; Table 1). *lep-5(fs19)* mutants replace 60 nt (G476-T535) with CA, eliminating the 3′ stem-loop and truncating ORF3, but leaving the other ORFs intact; these mutants phenocopy the *lep-5(ny28)* null allele (Figs. 2D, E; Table 1). Most tellingly, we created three mutants to disrupt the predicted central “zipper” and then restore it with predicted compensatory changes ~230 nucleotides away (Fig. 2D, E; Table 1). In *lep-5(fs21)*, six point mutations were introduced into the top strand of the zipper, dramatically weakening its potential to form a double-stranded region. These mutations also cause missense changes to putative ORFs 1 and 2. Separately, *lep-5(fs22)* introduced seven

point mutations into the lower strand of the zipper, similarly disrupting it; this causes five missense changes in ORF3. Both *lep-5(fs21)* and *lep-5(fs22)* mutants had completely penetrant TTM defects that phenocopy the *lep-5* null allele (Fig. 2E). Thus, *lep-5* function can be eliminated by two separate mutants that disrupt a central secondary-structure feature but cause no common lesion to putative coding sequence. Finally, we introduced mutations equivalent to *fs22* into *fs21* to create the “double mutant” *fs21fs25*, which is predicted to restore the secondary structure of the *lep-5* RNA but leave extensive coding sequence changes in all putative ORFs (Fig. 2D). Strikingly, *lep-5(fs21fs25)* mutant males are phenotypically wild-type (Fig. 2E; Table 1). Thus, the integrity of the central “zipper” region of *lep-5* RNA is essential for its function, and overwhelming evidence indicates that *lep-5* activity is independent of the coding potential of its ORFs.

Consistent with an RNA-based function for *lep-5*, several previous studies have found the *lep-5* RNA in ribonucleoprotein complexes *in vivo*. Two regions of *lep-5*, C335-G392 and T415-A467, were identified in CLIP-seq experiments with the Argonaute ALG-1 (Grosswendt et al., 2014). Another region, A531-T551, was suggested to interact with the Dicer DCR-1 (Rybak-Wolf et al., 2014). Note that Dicer can bind to many classes of RNA, including lncRNAs and mRNAs, and that this interaction does not necessarily imply cleavage (Rybak-Wolf et al., 2014). In HITS-CLIP experiments, *lep-5* was found to interact with the heterochronic factor LIN-28, also through a region in its 3' end (G434-G584) (Stefani et al., 2015).

Because of the extensive involvement of miRNAs in *C. elegans* developmental timing (Abbott et al., 2005; Lee et al., 1993; Reinhart et al., 2000), and because of *lep-5*'s association with ALG-1 and DCR-1, we considered the possibility that the full-length *lep-5* transcript might serve as a precursor for one or more smaller RNAs. However, deep sequencing from multiple stages and both sexes in *C. elegans* has identified no small RNAs derived from this region (Gerstein et al., 2010; Kato et al., 2009), despite high abundance of the full-length *lep-5* RNA. These results cannot exclude the possibility that very low-abundance, temporally regulated, or unstable miRNAs might be made from the *lep-5* locus. However, the structure-function experiments above, together with results detailed below, are more consistent with a lncRNA-based function for *lep-5*.

***lep-5* lncRNA is expressed in a temporal wave and localizes to the cytoplasm**

To examine the *lep-5* expression pattern, we fused ~4 kb of upstream sequence to GFP. This *Plep-5::GFP* reporter was expressed in larvae of both sexes in several cell types including the tail tip, pharynx, nervous system, vulva, and seam cells (Fig. 3A, Fig. S6). Notably, expression of the reporter was temporally controlled: GFP was first weakly detectable in early L2, became stronger in late L2 and persisted until late L3. Expression was weak in L4 animals and nearly undetectable in adults. By qRT-PCR, *lep-5* abundance showed a similar pattern, with expression low during L1 but rising dramatically by late L2 and remaining high through early L4 (Fig. 3B). *lep-5* levels were markedly reduced in *lep-5(fs8)* mutants (Fig. 3B), suggesting that the 5' stem-loop is important for RNA stability. SL1-trans-spliced *lep-5* transcripts were still detectable in *lep-5(fs8)* mutants (not shown), indicating that the *fs8*

mutation does not abolish trans-splicing, though it is possible that such processing is impaired.

To determine the subcellular localization of the *lep-5* lncRNA, we carried out single molecule fluorescent *in situ* hybridization (smFISH). *lep-5* RNA was readily detectable in the tail tip of an L2 male (Fig. 3C, D). Co-staining with DAPI indicated that *lep-5* RNA is predominantly, if not exclusively, cytoplasmic. Consistent with the broad expression of the transcriptional reporter, *lep-5* RNA was also detectable throughout the body, including neuronal ganglia of the head and tail (Fig. 3E, F) and in the developing male somatic gonad (Fig. 3G).

lep-5* is necessary for timely activation of the master TTM regulator *dmd-3

TTM is initiated by male-specific expression of the *doublesex* ortholog *dmd-3* in the tail tip (Mason et al., 2008). *dmd-3* expression follows a characteristic temporal pattern, with expression first detectable in the tail tip cells in early L4 (Fig. 4A) (Mason et al., 2008). By late L4, TTM is complete and tail tip expression of *dmd-3* becomes undetectable. In *lep-5(ny10)* L4 males, *dmd-3* expression was absent in the tail tip cells, while in *lep-5(fs8)*, it was variably lost and delayed (Fig. 4A and data not shown). Moreover, many *lep-5* males showed aberrant expression of *dmd-3* in adulthood (Fig. 4A), likely accounting for the adult activation of TTM described above (Fig. 1H). Thus, *lep-5* regulates the timing of TTM by controlling the temporal dynamics of *dmd-3* expression in the tail tip.

***lep-5* acts in the heterochronic pathway**

The altered timing of TTM in *lep-5* mutants, as well as the supernumerary molts and hermaphrodite alae defects, led us to consider whether *lep-5* might act in the *C. elegans* heterochronic pathway (Rougvié and Moss, 2013). Consistent with this, we found that passage through the dauer stage, an L3 alternative used in times of stress, strongly suppressed the morphogenesis defect of *lep-5* males (Table 1, Fig. 4B). Suppression by dauer is a characteristic feature of several heterochronic mutants (Liu and Ambros, 1991). Furthermore, the phenotype of *lep-5(ny10)* mutants was enhanced by RNAi knockdown of the RISC component *ain-1*, which by itself causes only weak heterochronic defects but modifies the phenotypes of many heterochronic mutants (Ding et al., 2005). While *ain-1(RNAi)* males had no male tail defects, all *ain-1(RNAi); lep-5(ny10)* males displayed severe defects in anterior tail retraction and TTM ($n = 28$, Fig. S1). *ain-1(RNAi)* also strongly enhanced the frequency of supernumerary molts of *lep-5(ny10)* adults to 100% in both sexes ($n > 20$). However, we observed no effect of *ain-1* RNAi on seam cell development in *lep-5* mutants, as all *ain-1(RNAi); lep-5(ny10)* adults had a normal number of seam cells ($n = 27$), which fused normally ($n = 67$), and males had normal alae ($n = 38$). Together, these findings indicate that *lep-5* is a component of the heterochronic pathway.

We carried out several experiments to determine the regulatory relationships between *lep-5* and other heterochronic genes. *let-7* and its key target, the NHL/TRIM gene *lin-41*, regulate the timing of TTM (Del Rio-Albrechtsen et al., 2006; Mason et al., 2008). We found that *lin-41(lf)* and *lin-41(RNAi)* suppressed the *lep-5* TTM phenotype (Table 1; Figs. 4B, C). Moreover, *Plin-41::GFP::lin-41 3'UTR* expression, normally downregulated during L4,

persisted into adulthood in *lep-5* mutants (Fig. S7). These observations indicate that *lep-5* functions upstream of *lin-41*. Furthermore, five-fold overexpression of *let-7* via the transgene *zals3* (Bussing et al., 2010), while causing no tail tip phenotype in a wild-type background, was able to almost completely suppress the *lep-5* mutant phenotype (Figs. 4B, C). Thus, *lep-5* likely acts upstream of *let-7*.

The RNA-binding protein LIN-28 acts upstream of *let-7* and is a central regulator of developmental progression across species. In both *C. elegans* and mammals, a key role of LIN-28 is to repress the biosynthesis of mature *let-7* (Tsalikas and Romer-Seibert, 2015). Consistent with the precocious developmental phenotypes of *lin-28* mutants (Ambros and Horvitz, 1984; Vadla et al., 2012), these animals exhibit premature TTM (leading to over-retraction; Ore) (Herrera et al., 2016). We observed an Ore phenotype in many *lin-28(RNAi)* males and found that *lin-28(RNAi)* also strongly suppressed the *lep-5* TTM phenotype (Figs. 4B, C). Here, residual *lin-28* activity may prevent complete suppression, as the penetrance of the *lin-28(RNAi)* TTM phenotype indicates incomplete knockdown (Herrera et al., 2016). These results suggest that *lep-5* is a negative regulator of *lin-28*. Earlier in development, the transcription factor LIN-14 controls the progression between L1 and L2 stages by activating *lin-28* (Seggerson et al., 2002). Consistent with previous findings (Herrera et al., 2016), *lin-14(RNAi)* males also precociously retracted their tail tips, but *lin-14(RNAi)* had no effect on TTM in *lep-5(ny10)* mutants (Figs. 4B, C). Together, these experiments support a model in which *lep-5* functions in the heterochronic pathway downstream of *lin-14* and upstream of *lin-28* and *let-7*.

***lep-5* is required for the timely decay of LIN-28**

Normal progression through larval development requires the downregulation of LIN-28 by the L3 stage (Moss et al., 1997). This allows the production of mature *let-7* miRNA and has other, *let-7*-independent, consequences (Vadla et al., 2012; Van Wynsberghe et al., 2011). Previous work has demonstrated that the control of *lin-28* mRNA stability and translation, mediated through its 3' UTR, is an important contributor to LIN-28 downregulation (Morita and Han, 2006). To ask if *lep-5* has a role in this process, we examined LIN-28 protein levels by Western blot (Fig. 5A). As expected, LIN-28 abundance in wild-type larvae was high in L1 and decreased significantly by L3. In *lep-5* mutants, LIN-28 levels were similar to those seen in wild-type during L1, but were markedly elevated in L3, indicating a defect in LIN-28 downregulation. By qRT-PCR, however, we found that the loss of *lep-5* had no effect on *lin-28* mRNA abundance in L3 (Fig. 5B). Thus, *lep-5* is necessary for the developmental decline in LIN-28 protein, but it does not affect *lin-28* mRNA levels. Consistent with this function, we found that overexpression of a LIN-28::GFP fusion protein in *lep-5* mutants, but not in wild type, caused lethality due to highly penetrant supernumerary adult molts in both sexes (data not shown).

Given these results, we considered two models for *lep-5*-mediated regulation of *lin-28*. First, *lep-5* might be important for repressing translation of *lin-28* mRNA. Such a mechanism is used by the heterochronic genes *daf-12*, *lin-66*, and *sea-2*, which repress *lin-28* translation through its 3' UTR (Huang et al., 2011; Morita and Han, 2006; Seggerson et al., 2002). Alternatively, *lep-5* could promote the degradation of LIN-28 protein between L1 and L3. To

distinguish between these possibilities, we used a photoconvertible LIN-28::Dendra2 fusion protein to monitor the stability of LIN-28 protein during development (Herrera et al., 2016). As expected, LIN-28::Dendra2 abundance was high in L2 animals, and UV illumination converted essentially all of this fusion protein from green to red (Fig. 5C). When these animals reached early L4, the pool of pre-existing (red) LIN-28::Dendra2 was nearly undetectable, and we observed no newly synthesized (green) LIN-28::Dendra2. In *lep-5* mutants, LIN-28::Dendra2 levels were comparable to wild-type at the L2 stage, consistent with our Western blot results. Similarly, very little newly synthesized (green) LIN-28::Dendra2 was detectable in early L4 following photoconversion in L2. However, unlike wild-type larvae, *lep-5* mutants exhibited significant amounts of pre-existing (red) LIN-28::Dendra2 protein in L4. Thus, the pool of LIN-28::Dendra2 synthesized before photoconversion was markedly more stable in *lep-5* mutants than in wild type. This indicates that *lep-5* regulates developmental timing by promoting the timely degradation of LIN-28 protein.

lep-5* RNA associates with LIN-28 and LEP-2 *in vivo

lep-2, another recently identified heterochronic gene, shares many phenotypic similarities with *lep-5* (Herrera et al., 2016). Both mutants have severe TTM defects, both genes act in the heterochronic pathway, and both are required for the timely degradation of LIN-28. *lep-2* encodes the sole *C. elegans* Makorin, a conserved but poorly understood family of proteins with RNA-binding and E3 ubiquitin-ligase capacities (Cassar et al., 2015; Gray et al., 2000; Kim et al., 2005; Lee et al., 2012; Lee et al., 2009; Liu et al., 2017a; Salvatico et al., 2010). Correspondingly, Herrera et al. (2016) hypothesized that LEP-2 might act as the E3 ligase that tags LIN-28 for proteasomal degradation. Because both LIN-28 and LEP-2 are RNA-binding proteins, we considered the possibility that they might both bind to *lep-5*.

We therefore immunoprecipitated *in vivo*-crosslinked RNA-protein complexes to ask if LEP-2 and LIN-28 bound specifically to the *lep-5* RNA. Using animals carrying a functional GFP::LEP-2 transgene, we carried out anti-GFP immunoprecipitation to recover GFP::LEP-2 along with any covalently-bound RNAs. After washing and crosslink reversal, we measured the recovery of *lep-5* RNA and a control mRNA expressed at similar levels, *cdc-42*, by qRT-PCR and compared these to the recovery from negative-control (empty beads) immunoprecipitations. We robustly detected *lep-5* RNA in the GFP::LEP-2 immunoprecipitate, while *cdc-42* RNA was present only in trace amounts (Fig. 5D). Using a similar approach, we isolated RNAs associated *in vivo* with GFP::LIN-28 and with a negative control RNA-binding protein, GFP::LIN-41. Again, we found *lep-5* RNA, but not significant amounts of *cdc-42* RNA, in association with GFP::LIN-28. In contrast, negligible amounts of both RNAs were recovered in GFP::LIN-41 complexes (Fig. 5D). Together, these results demonstrate that LIN-28 and LEP-2 bind specifically to *lep-5* RNA *in vivo*, suggesting that *lep-5* might act as an RNA scaffold in a tripartite LEP-2—*lep-5*—LIN-28 complex that mediates the degradation of LIN-28.

DISCUSSION

Here, we report the discovery of a *C. elegans* lncRNA, *lep-5*, and demonstrate that it regulates the timing of two events in the juvenile-to-adult transition: male tail morphogenesis and the final molt. *lep-5* functions upstream of *lin-28*, a central regulator of developmental transitions—including the juvenile-to-adult transition—throughout the animal kingdom. *lep-5* promotes the timely degradation of LIN-28, an essential step for properly coordinated larval development. This regulation is likely direct and might reflect a scaffolding ability of *lep-5*, through which it may promote LIN-28 proximity to an E3 ligase, LEP-2, whose mutant phenotype is nearly identical to that of *lep-5*. The *lep-5* lncRNA is found in the cytoplasm, where LIN-28 and LEP-2 are localized and predicted to be active (Herrera et al., 2016), thus adding an important regulator to the small list of known cytoplasmic lncRNAs. To date, few lncRNAs have been characterized in *C. elegans*: *rncs-1* is thought to play a role in the response to starvation (Hellwig and Bass, 2008), and *tts-1* regulates ribosome levels to promote the extended lifespan of insulin receptor mutants (Essers et al., 2015). A recent study identified behavioral and developmental phenotypes for 23 putative *C. elegans* lncRNAs, finding that most appear to regulate transcription or bind to endogenous miRNAs (Wei et al., 2019). These studies did not include *lep-5*, as H36L18.2 was not originally annotated as a predicted lncRNA. Our findings that *lep-5* acts cytoplasmically to regulate LIN-28 stability highlight the extensive use of non-coding RNA in the heterochronic pathway.

***lep-5* is a lncRNA component of the *C. elegans* heterochronic pathway**

The delay of TTM, the presence of supernumerary molts and partially defective alae, the suppression by passage through dauer, and the enhancement by *ain-1(RNAi)* suggest that *lep-5* functions in the heterochronic pathway. The finding that *lep-5*'s key function is to promote the timely degradation of LIN-28 provides a straightforward mechanism to explain the Lep defect. Perdurance of LIN-28 function would block biogenesis of the mature *let-7* miRNA (Tsialikas and Romer-Seibert, 2015), which would then be unable to downregulate its target *lin-41*. Because *lin-41(gf)* blocks *dmd-3* activation and the onset of TTM (Del Rio-Albrechtsen et al., 2006; Mason et al., 2008), the persistence of *lin-41* in *lep-5* mutants accounts for these heterochronic defects. That *lep-5* mutants do not completely phenocopy some other mutants that disrupt LIN-28 degradation—particularly with respect to defects in seam cell lineages—strongly suggests cell-type-specificity in the control of LIN-28 (see below). We believe that *lep-5* provides an instructive temporal cue for TTM, as overexpression of wild-type *lep-5* is sometimes sufficient to cause premature morphogenesis (Ore) (Fig. 2C).

While multiple genes have been shown to be necessary for the proper temporal decline in *lin-28* activity, many of these (e.g., *lin-4*, *lin-66*, *daf-12*, and *sea-2*) function through the 3' UTR of *lin-28* to repress its translation (Hochbaum et al., 2011; Huang et al., 2011; Morita and Han, 2006; Moss et al., 1997). In contrast, *lep-5*, like *ced-3* and *lep-2* (Herrera et al., 2016; Weaver et al., 2014), acts to promote LIN-28 protein degradation. The caspase CED-3, a protease best known for its role in programmed cell death, can act directly on LIN-28

(Weaver et al., 2017; Weaver et al., 2014). The Makorin LEP-2, as a putative E3 ligase, may promote LIN-28 degradation via ubiquitination (Herrera et al., 2016).

***lep-5* may act as a molecular scaffold**

How could the *lep-5* lncRNA regulate LIN-28 stability? In other systems, many functional roles for lncRNAs have been described, especially the regulation of transcription or chromatin state of nearby genes (Fatica and Bozzoni, 2014; Geisler and Coller, 2013). We considered such a function for *lep-5* but found no obvious nearby candidate target genes. Moreover, the cytoplasmic localization of *lep-5* RNA makes this possibility unlikely. Many lncRNAs function by direct base-pairing to other RNAs (Cech and Steitz, 2014; Fatica and Bozzoni, 2014; Kretz et al., 2013), but *lep-5* has no significant complementarity to any known transcribed regions of the *C. elegans* genome (BlastN e-values > 0.3) and it does not harbor a target site for a relevant miRNA (see STAR Methods).

lncRNAs can also function as molecular scaffolds by recruiting factors into a functional complex (Ransohoff et al., 2018; Wang and Chang, 2011). Our results favor this hypothesis for *lep-5*. By immunoprecipitation of intact ribonucleoprotein complexes, we found that both LIN-28 and LEP-2 bind to *lep-5* *in vivo*. LIN-28 possesses two RNA binding domains (Tzialikas and Romer-Seibert, 2015) and can bind RNA directly (Van Wynsberghe et al., 2011). In previous HITS-CLIP experiments, *lep-5* was found among the ~2000 RNA species that interact with LIN-28 *in vivo* (Stefani et al., 2015). LEP-2 is the sole *C. elegans* Makorin (Herrera et al., 2016), a family of conserved proteins that can bind nucleic acids and act as E3 ubiquitin ligases (Arumugam et al., 2007; Gray et al., 2000; Lee et al., 2009; Liu et al., 2017a; Salvatico et al., 2010). Because both *lep-5* and *lep-2* facilitate the degradation of LIN-28, we propose that the key function of *lep-5* is to scaffold a tripartite LEP-2-*lep-5*-LIN-28 complex. As such, *lep-5* would provide an instructive switch, allowing LEP-2 to act on LIN-28, causing it to be ubiquitinated and ultimately degraded by the proteasome (Fig. 6). Such a mechanism would be similar to that of HOTAIR, an lncRNA that unites RNA-binding E3 ligases with their substrates (Yoon et al., 2013). Once LIN-28 levels decline, *pre-let-7* is able to be processed by Dicer, and the resulting increase in mature *let-7* miRNA promotes the juvenile-to-adult transition. This model accounts for the phenotypic similarity between *lep-2* and *lep-5*, and explains why LEP-2, despite being nearly ubiquitously present from embryo to adult, is apparently only active during the period when *lep-5* is expressed (Herrera et al., 2016). Intriguingly, Argonaut binding is suggested to be involved in destabilizing HOTAIR RNA (Yoon et al., 2013), which, given the potential binding of ALG-1 to *lep-5* (Grosswendt et al., 2014), could also be the case here. Such predictions will be the focus of future work.

Cell-type specificity in developmental timing mechanisms

In contrast to their roles in the timing of TTM and the cessation of molting, neither *lep-5* nor *lep-2* (Herrera et al., 2016) is required for stage-specific patterns of seam cell division or their terminal differentiation and fusion, both of which are canonical aspects of heterochronic control (Rougvie and Moss, 2013). This separation of phenotypes indicates that there may be cell-type specific characteristics of heterochronic regulation. This idea has precedent: *lin-29*, the terminal regulator of the larval-to-adult switch in seam cells, is not

required for TTM (Ambros and Horvitz, 1984; Del Rio-Albrechtsen et al., 2006). Instead, *dmd-3* fulfills this role (Mason et al., 2008). Nevertheless, given that *lep-5* acts upstream of *lin-28*, it is surprising that *lep-5* mutants display no strong defects in the seam. One possibility is that cell-type-specific mechanisms are important for regulating *lin-28* activity. Additionally, different tissues may differ in their thresholds for *lin-28* activity, such that the seam might be less sensitive and tail tip and body hypodermis (*hyp7*) more sensitive to increased *lin-28* function. In any case, the identification of *lep-5* and *lep-2* indicate that the male tail tip provides an important and sensitive read-out for studies of the heterochronic pathway, key aspects of which could be missed by focusing exclusively on seam cells. Additionally, cell-type-specific variation in the heterochronic pathway could provide important developmental and evolutionary flexibility. Indeed, tissue-specific changes in developmental timing ("heterochrony") are thought to have important roles in morphological evolution (Gould, 1977).

Structural features of *lep-5* RNA

The predicted secondary structure of *lep-5* features extensive base-pairing, indicating that its higher-order structure is important for its activity. Disrupting the secondary structure of the central zipper as well as the 5' stem-loop *in vivo* completely eliminated *lep-5* function; restoring secondary structure with complementary mutations restored function. Interestingly, the predicted stem-loop at the 5' end includes the trans-spliced leader SL1. While SL1 is speculated to promote translation initiation of *C. elegans* mRNAs (Blumenthal, 2005), our results indicate that SL1 can also have a role in RNA secondary structure and lncRNA function. The 5' stem-loop might be an important binding site for *lep-5* interactors; it is also important for RNA stability, as *lep-5* levels were reduced ~5-fold in *lep-5(fs8)* mutants.

lep-5 lncRNA directly interacts with LIN-28 and LEP-2/Makorin. Both proteins—and even their roles in regulating developmental transitions, including the juvenile-to-adult transition—are highly conserved in animals (Abreu et al., 2013; Faunes et al., 2017; Faunes and Larrain, 2016; Gray et al., 2000; Herrera et al., 2016; Thornton and Gregory, 2012). Although one might expect this conservation to extend to *lep-5*, we did not find homologs outside of *Caenorhabditis*. It seems unlikely that *Caenorhabditis* evolved a special lncRNA-mediated mechanism to catalyze the LIN-28 degradation that must occur in all animals. Rather, we propose that the *lep-5* primary sequence evolves rapidly and is therefore difficult to detect in more distantly related species by sequence similarity. Even identifying the *C. angaria lep-5*—which rescued *C. elegans lep-5* mutants—required synteny and bioinformatic analyses in addition to BlastN (see STAR Methods). In general, lncRNAs are known to evolve rapidly, and orthologs of many functionally important lncRNAs are not easily found outside closely related species (Diederichs, 2014). One explanation is that functional conservation in some lncRNAs may depend more on 3D structure than primary sequence. Considering this and the conservation of the *LIN28-let-7* regulatory module (Tzialikas and Romer-Seibert, 2015), we propose that *lep-5* orthologs could indeed exist in other species but might not be identifiable based on sequence alone. Notably, recent work has shown that several lncRNAs are important for pluripotency and differentiation in mammalian stem cell systems (Flynn and Chang, 2014); the same biological processes often feature regulation by *LIN28-let-7* (Shyh-Chang and Daley, 2013). Indeed, a recently

identified rodent-specific lncRNA, *Ephemeron*, modulates the exit of embryonic stem cells from pluripotency by regulating Lin28a; however, unlike *lep-5*, *Ephemeron* promotes Lin28a expression (Li et al., 2017). Several lncRNAs have also been implicated in the regulation of LIN28 in cancer cells, in some cases through a feedback loop involving let-7-family miRNAs (Gao et al., 2017; He et al., 2018; Peng et al., 2017; Wang et al., 2016). Our results in *C. elegans* indicate that lncRNA regulation of *lin-28* is an anciently conserved component of mechanisms that control cell state changes and developmental progression.

STAR METHODS

CONTACT FOR REAGENT AND RESOURCE SHARING

Further information and requests for resources and reagents should be directed to and will be fulfilled by the Lead Contact, Douglas Portman (douglas.portman@rochester.edu).

EXPERIMENTAL MODEL AND SUBJECT DETAILS

These studies used the nematode *C. elegans*, which was cultured as described by Brenner (1974). Most experiments were carried out on larval and adult males, as these studies focus on a male-specific morphogenetic process. Most strains used here contained the mutation *him-5(e1490)*, which increases the frequency of spontaneous XO males among the self-progeny of XX hermaphrodites.

METHOD DETAILS

Microscopy and phenotypic analysis—For microscopy, worms were placed in a drop of 20 mM sodium azide or 1 mM levamisole on 5% agar pads and studied at 400x or 1000x magnification with a Zeiss Axioskop with Nomarski (DIC) and epifluorescence. Images were recorded with a C4742-95 “Orca” Hamamatsu digital camera and Openlab software, ver. 3.0.9 (Improvision). Confocal images were obtained with a Leica TCS SP8 X microscope using the 63x objective. Images were taken as Z-stacks with 0.5 or 1 μ m steps. Simple image editing was performed with ImageJ. To investigate cell-fusion phenotypes caused by *lep-5* mutations and assess the number of seam cells in adult animals, we examined strain DF235 carrying the *lep-5(ny10)* mutation, the adherens junction reporter AJM-1::GFP (Koppen et al., 2001), and the seam cell reporter pF09D12.1::GFP.

Isolation and mapping of *lep-5* mutants—The *lep-5(ny10)* deletion allele was isolated in a screen for Lep male phenotypes in which CB4088 hermaphrodites were mutagenized with trimethylpsoralen (TMP) and exposure to UV light. Using competitive genome hybridization (CGH), we identified two large deletions on X in *lep-5(ny10)* genomic DNA (see below; Fig. S2A). *lep-5(fs8)* was isolated in a mutagenesis screen in which *bxIs14 him-5(e1490)* hermaphrodites were mutagenized with ethylmethanesulfonate (EMS). In both screens, F1 hermaphrodites were isolated to produce the F2 generation, which were segregated. F3 male progeny of individual F2s were scored at 400x magnification for defects in ray development and tail tip morphology. Mutants were outcrossed several times with CB4088 to generate the strains used here. By SNP mapping, *fs8* was found to lie in a 2.7-Mb region that was deleted in *ny10*.

A fosmid covering one end of the *ny10* deletion rescued the *lep-5* phenotype; subsequent truncations of this region indicated that a ~3 Kb fragment containing the predicted gene H36L18.2 was sufficient for rescue (Figs. S2B, C). By sequencing *lep-5(fs8)*, we identified a single G-to-A change (G23A) in the first nucleotide following the SL1 trans-splicing acceptor site (Fig. S2C). Introducing this mutation into the 3-Kb rescuing fragment markedly reduced its activity (Fig. 2B). Together, these results indicate that *lep-5* corresponds to H36L18.2.

Array comparative genomic hybridization to map deletions in *lep-5(ny10)*—The *ny10* allele of *lep-5* was mapped by comparative genomic hybridization by Nimblegen (Roche). Genomic DNA was isolated from the *lep-5* mutant (strain DF70) and the wild type reference strain (CB4088) using the Gentra Puregene Tissue Kit (Qiagen). The tiling arrays contained 385,179 probes with a median spacing of 167 nt covering the whole *C. elegans* genome. Reference and mutant DNA were differentially labeled with Cy3 or Cy5 dye and hybridized to the tiling array. The fluorescence intensity for Cy3 and Cy5 was measured at each probe position and the expression values were log₂-normalized. To visualize the tiling array data, the ratio of the normalized expression values for each probe was plotted according to its position within the *C. elegans* genome (Fig. 2A). We detected a ~24.6kb deletion on the left arm of ChrX (6,554,074 to 6,578,133 bp) and an ~86kb deletion on the right arm of ChrX (12,576,888 to 12,662,886 bp). To separate the deletions, we performed crosses with a strain that carries *unc-18* and *dpy-6* mutations between the deletions (EM122). Recombinant Dpy nonUnc or nonDpy Unc hermaphrodites were isolated and their male progeny screened for tail tip phenotypes. The Lep phenotype was only found in nonDpy Unc males, demonstrating that the *lep-5* lesion was located on the right arm of ChrX. The *lep-5(ny10)* mutant was backcrossed to CB4088 multiple times, resulting in the homozygous strain DF135.

Complementation tests to show that *fs8* and *ny10* are allelic—Because *lep-5* is located on the X chromosome and the Lep phenotype is only observed in males, we used XX pseudomales to test whether *lep-5(ny10)* and *fs8* are dominant or recessive mutations and for genetic complementation of the two alleles. First, males from a *tra-1(e1488)III; him-5(e1490)V* strain were crossed with hermaphrodites from a *him-5(e1490)V; unc-18(e81) lep-5(ny10)X* strain. nonUnc F1 hermaphrodites were allowed to self and the nonUnc F2 pseudomales were scored for tail tip phenotypes. All of these animals had wild-type tails, demonstrating that *lep-5(ny10)* is recessive. The Unc F2 progeny from this cross were used to establish a *tra-1; him-5; unc-18 lep-5(ny10)* strain. Hermaphrodites with this genotype were then crossed with post-dauer *lep-5(fs8)* males. nonUnc F1 hermaphrodites were allowed to self. If *fs8* and *ny10* were non-allelic, only 1/3 of the of the Tra nonUnc F2 pseudomales should display the Lep phenotype. We examined 79 such animals and found that all were Lep, indicating that both alleles are mutations in the same gene. To exclude that the proportion of homozygous *fs8* pseudomales was significantly distorted by the X chromosome non-disjunction in oocytes due to the *him-5* mutation in the background of all strains, we followed the progeny of these hermaphrodites; 48 animals were sterile, 10 gave only nonUnc progeny (and were therefore homozygous for *fs8*). 21 yielded F3 progeny of

which 25% were Unc, confirming that these animals were indeed heterozygous for *fs8* and *ny10*. We concluded that *ny10* and *fs8* are alleles of *lep-5*.

Transgenesis—Transgenes for rescue experiments and expression constructs were made by overlap extension PCR (Nelson and Fitch, 2011) or by modification of plasmids using site directed mutagenesis. PCR products used for transgenesis were gel-purified with the Promega Wizard[®] SV Gel and PCR Clean-Up System. Unless otherwise noted, we used the pRF4[*rol-6(d)*] plasmid at a concentration of 100ng/μl as injection marker. PCR products were microinjected at a concentration of 0.5 or 1ng/μl into the gonads of young hermaphrodites. Sequences of oligos used to generate DNA constructs for transgenesis are listed in Table S1.

Fosmid and PCR rescue—Bacteria containing Geneservice fosmid clones WRM062bG06, WRM0629cE12, WRM0628aE08 and WRM0640cA10 were grown according to the company's protocol. Fosmid clones were amplified using Epicentre CopyControl induction solution and isolated with the QIAprep Spin Miniprep kit (Qiagen). The fosmid identities were verified by sequencing (pCC1-forward). Fosmids were then linearized by digestion with SfiI, purified with QIAquick spin columns and injected into *lep-5(ny10)* hermaphrodites at a concentration of 4nμl. Fosmids were injected in groups of two or separately and transgenic males scored for rescue of the Lep phenotype. WRM0640cA10 was the only fosmid that rescued. Sections of its sequence, covering one or two predicted genes were generated by PCR and injected at a concentration of 1ng/μl. A 6506nt long PCR product obtained with primers H36L18.2_F and H36L18.2_R and covering the gene H36L18.2 rescued the phenotype of *lep-5(ny10)*. To determine the minimal rescuing fragment for *lep-5*, subsequently smaller PCR products were injected into *lep-5(fs8)* mutants with *Punc-122::GFP* as injection marker.

Transgenes with secondary structure modifications of *lep-5*—Six different transgenes covering 3133 nt of the *lep-5* transcribed and upstream sequence were made by PCR and injected into the gonads of *lep-5(ny10)* hermaphrodites at a concentration of 0.5 or 1 ng/μl. At least 4 lines were scored for each experiment.

(1) *lep-5(+)* PCR fragment was amplified from N2 genomic DNA with primers KKlp5_expr-9 and KKlp5_expr-10.

(2) *lep-5(G23A)* PCR fragment was amplified from genomic DNA of *lep-5(fs8)* mutants with primers KKlp5_expr-9 and KKlp5_expr-10. Because the *lep-5(fs8)* mutation is temperature-sensitive and the construct *lep-5(G23A)* showed some degree of rescue when injected at 1ng/μl, we also injected it at a ten-fold concentration.

Four transgenes were made by overlap extension PCR using N2 genomic DNA as template. The modifications noted were introduced into the reverse primer of the first PCR product (A piece) and the forward primer of the second PCR product (B piece). The final product was amplified with primers KKlp5_expr-9 and KKlp5_expr-10.

(3) *lep-5*(G23A, C30T). Primers for A piece (forward and reverse): KKlp5_expr-1 and KKlp5_23A+30T-R. Primers for B piece: KKlp5_23A+30T-F and KKOLp5-8a.

(4) *lep-5*(G23C). Primers for A piece: KKlp5_expr-1 and KKlp5_23C_R. Primers for B piece: KKlp5_23C_F and KKOLp5-8a.

(5) *lep-5*(G23C, C30G). Primers for A piece: KKlp5_expr-1 and KKlp5_23C+30G-R. Primers for B piece: KKlp5_23C+30G-F and KKOLp5-8a.

(6) *PCel-lep-5::Cbr-lep-5(+)*. Primers for A piece (forward and reverse): KKlp5_expr-1 and KKlp5_Cbr-AR used on N2 DNA; Primers for B piece: KKlp5_Cbr-BF and KKOLp5-8a used on *C. briggsae* PB800 DNA. The final product was amplified with KKlp5_expr-9 and KKlp5_Cbr-nR.

(7) *PCel-lep-5::Can-lep-5(+)*. Primers for A piece (forward and reverse): KKlp5_expr-1 and KKlp5_Can-AR used on N2 DNA; Primers for B piece: KKlp5_Can-BF and KKOLp5-8a used on *C. angaria* PS1010 DNA. The final product was amplified with KKlp5_expr-9 and KKlp5_Can-nR. All final products were sequenced with primer RHOLp5-2 to confirm the presence of the desired modification.

Transgenes with stop codons and deletions—Site-directed mutagenesis with QuikChangeXL (Agilent Technologies) was used to introduce stop codons into a plasmid containing the minimal rescuing fragment for *lep-5* following the manufacturer's instructions. This plasmid was generated by cloning a PCR product, made with attBlep-5F6 and attBlep-5R6, into the Gateway vector pDONRTMP4-PIR (Life Technologies). Primers AA4,5,7F and AA4,5,7R were used to convert amino acids 4, 5 and 7 of the predicted ORF of H36L18.2 into stop codons. Amino acids 14 and 15 were converted into stop codons using primers AA14,15F and AA14,15R. The resulting plasmids were sequenced to confirm the changes and injected into *lep-5(fs8)* hermaphrodites with *Punc-122::GFP* as injection marker.

To create deletion constructs, two PCR products, covering the minimal rescuing fragment for *lep-5* with a gap at the intended deletion were amplified with primers that introduced an AatII restriction site at the 3' end of the first and the 5' end of the second piece. The PCR products were digested with AatII, gel-purified and ligated with T4 DNA ligase. Replacement of the intended sequence by the 6-bp tag GACGTC was confirmed by sequencing. The constructs were injected into *lep-5(ny10)* hermaphrodites at a concentration of 10ng/μl with *Punc-122::GFP* as injection marker. The sequence cagtgaccataacaatgtatgcacaacctcttcggactttctcatctatggtggcgctg, containing an ALG-1 binding site (Zisoulis et al., 2010), was deleted with primer pairs lep-5F6 + 1R and 1F + lep-5R6. Sequence ttttcattattcattccaactcttaaatgataatcgaaaa, forming a predicted stem-loop, was deleted with primer pairs ep-5F6 + 2R and 2F + lep-5R6.

Genome editing using CRISPR/Cas9

ny28: To delete the endogenous *lep-5* locus, genome editing with CRISPR/Cas9 with *dpy-10* coCRISPR (Arribere et al., 2014) was performed as described in the protocol from

the Dernburg lab published on the Integrated DNA Technologies (IDT) website. Two guide RNAs were designed with ChopChop (Labun et al., 2016; Montague et al., 2014). The crRNAs, tracrRNA and CAS9 were purchased from IDT. The RNAs were reconstituted to a concentration of 200 μ M in the IDT duplex buffer. 1 μ l of each *lep-5*-specific crRNA and 2 μ l of tracrRNA and 1 μ l of *dpy-10* crRNA and 1 μ l of tracrRNA were mixed and incubated at 95°C for 5 minutes. RNA duplexes for *lep-5* and *dpy-10* were mixed 12:1 and diluted to 62 μ M. 0.5 μ l RNA duplex mix was mixed with 0.5 μ l of Cas9 enzyme and incubated at room temperature for 10 minutes. 1 μ l RNP complex was used for 10 μ l injection mix, supplemented with 0.2xTE buffer and 0.1 μ M single-stranded DNA oligo to edit the *dpy-10* locus. Young *him-5(-)* hermaphrodites were injected into both gonads and their offspring screened for the Rol and Dpy phenotype. Pools of 5 F1 hermaphrodites from plates with the most Rol and Dpy worms were screened for edits at the *lep-5* locus by PCR with primers KK_CR_lep-5_1 and KK_CR_lep-5_2. Several lines with deletion of the *lep-5* locus were obtained, one of which was retained (*lep-5(ny28)*). This allele deletes 572 nucleotides of the *lep-5* gene, from 104 nt upstream of the transcription start site through 468 nt of the transcript, replacing this region with 7 random nucleotides and leaving 59 nt at the 3' end.

fs18, fs19, fs21 and fs22: To modify the endogenous *lep-5* locus, CRISPR/Cas9 genome editing using *dpy-10* coCRISPR was performed as described (Arribere et al., 2014; Paix et al., 2015). One or two *lep-5* guide RNAs were designed with CRISPOR (Haeussler et al., 2016) and/or ApE software using the algorithm of Doench et al. (2014). The tracrRNA and crRNAs were purchased from Dharmacon. ssODNs and primers were made by IDT. Recombinant Cas9 (25 μ g/ μ l) was prepared as described (Paix et al., 2015). tracrRNA was reconstituted at 4 μ g/ μ l with RNase-free Tris Buffer. Similarly, each crRNA was reconstituted at 8 μ g/ μ l with Tris Buffer. Each ssODN was dissolved in RNase-free water at 500 ng/ μ l. For microinjection mixtures, we followed the published protocol (Paix et al., 2015) strictly, except that the total volume of each mixture was halved from 20 μ l to 10 μ l. Microinjection mixtures were incubated at 37°C for 10 min before injection and used within 1h after preparation. Young *him-5(-)* hermaphrodites were injected and their F1s were screened for Rol, Dpy or DpyRol phenotype. Pools of 3 F1 hermaphrodites from plates with the most Rol and Dpy worms were screened for edits at the *lep-5* locus by PCR and restriction enzymes digest. For each allele, one or two lines were obtained and kept. All strains were backcrossed to N2 or *him-5(e1490)* at least four times. Fragments containing the entire *lep-5* gene, along with ~500 nt flanking regions, were confirmed by Sanger sequencing.

fs21 fs25: Molecularly, *fs25* and *fs22* are identical alleles of *lep-5*. To generate *fs21 fs25*, the injection mix used for *fs22* was injected into young *him-5/+ V; lep-5(fs21)/oxTi1015 X* hermaphrodites. Non-fluorescent offspring, which must be *lep-5(fs21)* homozygotes, were selected for future screening. Outcrossing and sequencing was done as for other *fs* alleles.

lep-5 transcriptional reporter—A GFP reporter construct driven by the *lep-5* regulatory region was generated by OES-PCR. Primers KKOLp5-1 and KKkp5-GFPA-R were used to amplify the region upstream of the transcription start of *lep-5* from N2 genomic DNA (piece A). This PCR product overlaps with piece B containing 4x NLS-GFP and the unregulated 3'

UTR of let-8583, generated with KKI_{p5}_GFPB-f and MN-lin-44_8 from Plasmid pPD122.13 (Andrew Fire Vector Kit, Addgene). The final product was amplified with primers RHOLp5-7 and MN-lin-44_9, gel-purified and injected into CB4088 hermaphrodites; 8 lines were obtained.

***lep-5* lncRNA expression via smFISH**—For smFISH, we used custom Stellaris probes from Biosearch Technologies specific for *lep-5* lncRNA (22 probes) labeled with Quasar570 (excitation 548nm, emission 566nm) and for *lin-44* (39 probes) labeled with Quasar670 (excitation 647nm, emission 670nm). The probes were designed by Biosearch Technologies. Sample preparation and hybridization were performed in tubes using a modification of the protocols by Ji and van Oudenaarden (2012) and the protocol provided by Biosearch Technologies. Briefly: mixed stage or synchronized L2 worms from strains CB4088 (WT) and DF135 (*lep-5(ny10)*) were collected, washed in M9 buffer and fixed in 4% paraformaldehyde in 1x PBS for 40 minutes at room-temperature. Fixed worms were washed twice with 1x PBS and transferred to 70% ethanol and kept on a rotating shaker at 4°C overnight. Worms were then washed with wash buffer (10% deionized formamide in 2x SSC) and hybridized in hybridization buffer (100mg/ml dextran sulfate and 10% formamide in 2x SSC) with 75nM *lin-44* probes and 250nM *lep-5* probes for 4 hours at 37°C in a hybridizer. The hybridization solution was washed off with wash buffer and the samples incubated in wash buffer for 30 minutes at 30°C. Worms were washed in 2x SSC and mounted in ProLong Gold with DAPI (Life Technologies) in imaging chambers as described by Ji and van Oudenaarden (2012). The slides were imaged on the DeltaVision Elite Imaging System using solid-state illumination with filters for DAPI, TRITC (with Quasar570 labeled probes) and Cy5 (with Quasar670 labeled probes). Images were recorded with an Evolve 512 EMCCD camera and processed using the softWoRx software package.

Sequences of the Stellaris RNA FISH probes

Probes for *lin-44*: aatcaaaaggagctgctcgc gttgaagagcagtcgattg ggccagggagcaaagaataa
 tgcgctgctgggatctcattc ttggccttagtggtgaac tgggcaaccctgtttcaaaa gagcacgtgaatgcagaaga
 gcatgccagttgaattgac attactgtacaggatgtgt ttctgaactcctcgaac gattcgcacagtttgaagt
 tcccattgctgaaatctcaa aatattccagctccgaac tcaataacggcgatcatgc gagaagactctcgaaaccc
 ggcatgagcagatgacaacg caatcgtcaatccatccttg attcatttgaccatctgg tgagtacatccgccaactc
 cgttatccgtgtgaaacac ttgtgagcagcttctgacta aacaaagtattaccgctcc cttcaaatgtgcttcca
 tcttttgatggccaatctc ggcattgcaggaagagatt tgacaagaaccggatactcc ttcggttccagcaagtttc
 atcggtaatgtgctcaaggc cgtgcatactttccactaa atcatccgatagacttgg aatccgctgctttaccac
 atccggagacgcttctaaat caactgatttgccttgcaa cttgggtatgcgtctcattc caacacagccgatcacaatc
 tcgtgacgaatgctgaatcc tcacagtcacacttcacacg cagattgcaacaccacacga gcatgttggatacaatcct
 tcccattacacgtggatc aaaattaggcttttcggcgg

Probes for *lep-5*: gcccatgtctttgggaaaac tggagagccaggcctaataat gtcataagacaatcgcgga
 gctatcatcccacttacgat tgttggttagcattacacc catcttgcacaacactggg tatttgatgggtgacatcgc
 acaccctaattgaactccaa gcataagcgaattgacgat atatggtctaacttccgct tatgcgctaacaagtacgg
 taataatgttgatggccacg accagctgtgtgtgatttt taaaacggaccacctagtgt gatagcagatccaattccg
 caacaaggcctgaggagga cagctttgatcagttacaa fatggtcactgatccaccag aagaggtgtgcatacattg
 ccatagatgcagaaaagtcc caataaccagatacagcgc cgggtccaacattcttaaat

Time-course of *lep-5* expression via qPCR—Staged animals were obtained with the hatch-off method (Pepper et al., 2003) and collected 0, 12, 15, 18, 22, 26 and 41 hours after hatching at 25°C and flash-frozen. RNA was extracted using a modification of the tissue protocol for the RNeasy micro kit from Qiagen. Frozen worms were ground with a plastic pestle fitting into a 500µl tube. When the worms began to thaw, the tube was dipped into liquid nitrogen to re-freeze. This process was repeated 5 to 6 times before buffer was added and the sample disrupted by passing it through a syringe needle. A DNase treatment was performed on-column. Wash-steps were performed according to the protocol. RNA was eluted with water and concentrations checked by NanoDrop (Thermo Scientific). cDNA was generated from 250ng total RNA using the double-primed RNA to cDNA EcoDry Premix (Takara/Clontech). qPCR was performed using the iQ SYBR Green Supermix with a two-step PCR protocol (3 min 95°C; 40× 10 sec 95°C, 60 sec 60°C; followed by melt curve analysis) on the CFX96 real time PCR detection system (BioRad). Y45F10D.4 served as reference gene (Hoogewijs et al., 2008) For primer sequences see Table S1. Unknowns were run in triplicates, standards in singles. Data were evaluated using the standard-curve method.

RNAi knockdown—RNA-interference was performed by feeding *E. coli* transformed with inducible RNAi vectors to mothers or larvae as previously described (Nelson et al., 2011). Bacterial strains for *lin-14* and *lin-41* RNAi were from the J. Ahringer library, and those for *lin-28* from the M. Vidal library (Source Bioscience). For *lin-14* RNAi, L4 hermaphrodites were treated and their male progeny scored as L3, L4 and adults for defects in tail tip morphogenesis. For *lin-28* and *lin-41* RNAi, L1 larvae were fed and scored as L4 and adults. Bacterial strain HT115 carrying the L4440 plasmid was used as negative control.

***lin-28* mRNA levels**—Staged WT (CB4088) and *lep-5(ny10)* animals were collected by 4h hatch-off. Some of the L1 were flash-frozen immediately, the rest was plated onto seeded plates and placed at 20°C. L3 larvae were collected and flash frozen 27 hours later. RNA extraction and cDNA synthesis (using 440ng RNA) were performed as described above. qPCR was performed with primers *lin-28_FW2* and *lin-28_RV2* and Y45F10D.4 as reference gene as above.

Western blot—Western blot analysis by SDS-PAGE was performed according to standard procedure. For the L1 sample, arrested L1s were placed on food and collected a few hours later. L3 samples were collected 24 hours after plating arrested L1s at 20°C. Animals were washed twice with PBS, frozen in liquid nitrogen and ground in the presence of a protease inhibitor (Halt, Pierce), SDS buffer was added. Samples were heated to 95°C for 10 minutes and centrifuged to pellet the insoluble fraction. An aliquot was kept for Bradford assay. Approximately 10-20 µg of total protein was loaded onto a 10% Bis-Tris Bolt gel (Invitrogen). After electrophoresis and transfer to a nitrocellulose membrane, the blot was incubated overnight at 4°C with a rabbit anti-LIN-28 polyclonal antibody (gift from E. Moss; 1:5,000 dilution) and a mouse anti-actin monoclonal antibody (Sigma; 1:5,000 dilution) as a loading control. The blot was incubated 45 minutes in the dark with fluorescent secondary antibodies (Licor; 1:25,000) and scanned on a Licor infrared fluorescence scanner.

Analysis of LIN-28 degradation—To observe LIN-28 dynamics in *lep-5* mutants, we used a *Plin-28::Dendra2::lin-28_3'UTR* reporter gene (Herrera et al., 2016). In the *lep-5* genetic background, this transgene caused bursting of hermaphrodites, and no stable line could be established. Therefore, hemizygous male cross-progeny of *him-5; nyEx56[Plin-28::Dendra2::lin-28_3'UTR]* males and *him-5; lep-5(ny10)* hermaphrodites were investigated. The fluorescence signal of the reporter was visualized with a confocal microscope (Leica, SP8) as described in Herrera et al. (2016): L2 stage animals were examined and fluorescence in the pharynx region was captured for the green and red channels by sequential scans. Dendra2 photoconversion was performed by exposing a section of the pharynx to brief flashes of 405 nm light in 10–20 slices with ten successive scans of the z-plane with short rest periods inbetween. Sequential z-stacks of the exposed region were taken for the red and green channel to record the post-photoconversion fluorescent signal. The animal was recovered onto a plate with food and kept at 20°C for 24 h. The worms (now L3) were remounted, and another sequential z-stack was recorded. The image stacks were analyzed with ImageJ.

RNA co-IP with LEP-2, LIN-28 and LIN-41—Worms were synchronized by L1 arrest and grown for 17 hours at 25°C to the L2 stage (DF237 carrying LIN-28::GFP and DF282 carrying GFP::LIN-41), or mixed stages were used (DF293 carrying GFP::LEP, DF302 carrying *plep-5::GFP*). Worms were washed twice in M9 buffer and irradiated in a BioRad crosslinker with 800 mJ/cm² at 254nm. UV-treated worms were washed once in lysis buffer (20 mM Tris/Cl pH 7.4, 150 mM NaCl, 5 mM MgCl₂, 0.5 % NP-40 Igepal), resuspended in an equal volume of lysis buffer supplemented with HALT protease inhibitor (Invitrogen), RNaseOUT (Thermo Fisher) and DTT and flash frozen in liquid nitrogen. At least three biological replicates were obtained for each genotype. The frozen worms were manually ground in Takara Biomasher tubes and lysed in 200µl lysis buffer supplemented with HALT protease inhibitor and RNaseOUT. IP was performed with Chromotek GFP-Trap MA and Chromotek binding control magnetic agarose beads according to the guidelines by the company: The beads were equilibrated in dilution buffer (20 mM Tris/Cl pH 7.4, 150 mM NaCl, 5 mM MgCl₂) and resuspended in dilution buffer supplemented with RNase OUT, DTT and 400µM vanadyl ribonucleoside complexes. 40–90µl lysate was added to each kind of beads and incubated for 60 minutes at 4°C while tumbling end over end. 20% of this volume (8 - 18µl) was set aside as input sample. Beads were washed twice with dilution buffer and twice with wash buffer (20 mM Tris/Cl pH 7.4, 250 mM NaCl, 1 mM MgCl₂, 0.025% SDS, 0.05 % NP-40 Igepal). Beads and input samples were then treated for 20 minutes with Proteinase K (100µl PBS with 1µl 10% SDS and 2.5% Proteinase K (Invitrogen)) at 65°C on a Thermomixer (Eppendorf) to reverse the crosslink and digest the proteins. RNA was extracted with Trizol and BCP, precipitated over night at –80°C after adding GlycobluTM (Ambion), sodium acetate and isopropanol. The pellet was washed once with 70% ethanol, air dried and resuspended in 44µl water. A DNase treatment with rDNase I (Ambion) was performed for 20 minutes at 37°C. The RNA was re-purified immediately using the Qiagen RNeasy Micro kit following the manufacturer's protocol. The RNA was eluted with 12µl water. 10µl RNA was used in a 20µl cDNA synthesis reaction with the Clontech/Takara double-primed EcoDry cDNA synthesis kit, 2pg luciferase control mRNA (Promega) was added to each reaction as a control for cDNA synthesis. The cDNA was

diluted 1:7 for qPCR on a BioRad CFX instrument using the BioRad iQ SYBR Green Supermix and primers for *lep-5*, *cdc-42* and luciferase. *cdc-42* was chosen as a control gene because it was present at similar levels as *lep-5* (i.e., in qPCR of the input sample, the Ct values for these genes differed by no more than 1.5 except in the LIN-41::GFP strain, which showed especially high levels of *lep-5*). All samples were run in triplicates. The results were evaluated using the Pfaffl Method (Pfaffl, 2001) with empirical efficiencies of 2 for luciferase, 1.98 for *lep-5* and 1.91 for *cdc-42*, comparing Ct values for GFP-trap beads (experiment) to binding control. Results for *lep-5* and *cdc-42* were normalized against the spiked-in luciferase to account for differences in the efficiency of the RT reaction. A moderated T-test implemented in the Limma package was performed to test for significance of the results. This test is specifically designed for expression analyses with small sample sizes (Ritchie et al., 2015).

Identification of *lep-5* orthologs from other *Caenorhabditis* species—Sequences of *lep-5* transcripts for *C. brenneri*, *C. elegans* and *C. japonica* were confirmed by ESTs in WormBase. Genomic *lep-5* sequences for 15 other *Elegans* supergroup species (Kiontke et al., 2011) were extracted from whole genomes (WormBase, and <http://caenorhabditis.org>) after BlastN search (Camacho et al., 2009). An unambiguous *lep-5* homolog was not identified in the *C. sp. 26* genome. All sequences contained two introns, which were edited out manually by assuming that their positions are homologous and that they bear the typical GT and AG motif at their 5' and 3' ends, respectively. No significant matches were found by BlastN alone in *Caenorhabditis* species outside of the *Elegans* supergroup. However, after multiple sequence alignment of a syntenic region in *C. angaria* and 7 *Elegans* supergroup species, we identified a sequence in the *C. angaria* genome with similarity to *lep-5*. A BlastN search subsequently yielded a partial *C. angaria lep-5* cDNA sequence that had been previously assembled from RNA-seq reads, as part of the *C. angaria* genome project (Mortazavi et al., 2010). This sequence was used to design internal primers, which together with a primer complementary to SL1 and an anchored oligo(dT) primer amplified two overlapping fragments of *lep-5* from *C. angaria* cDNA (made from total RNA with the double-primed RNA to cDNA EcoDry Premix by Takara/Clontech). The fragments were sequenced to identify the full *C. angaria lep-5* transcript. This transcript was used for a BlastN search of draft genome assemblies for *Caenorhabditis* species outside of the *Elegans* supergroup (available from the laboratory of Mark Blaxter at <http://download.caenorhabditis.org>). This yielded *lep-5* loci from *C. castelli*, *C. sp. 38*, *C. plicata*, and *C. virilis*, which we confirmed by BlastN with the *C. virilis lep-5* genomic region. We used MAFFT v7.266 (Katoh and Standley, 2013) (to align the predicted *lep-5* transcripts of 19 *Elegans* group species (Figure S1), our *lep-5* cDNA and genomic sequences from *C. angaria*, and the four *lep-5* genomic regions from non-*Elegans* group species. To maximize its accuracy and control the order of aligned sequences, MAFFT was run with the arguments '*--localpair --maxiterate 16 --inputorder*'. We manually edited the resulting alignment in Jalview 2.9.0b2 (Waterhouse et al., 2009) to remove trailing or poorly aligned flanking regions. Via the *hmmbuild* and *hmmsearch* programs from HMMER 3.1b2 (Eddy, 2011), we converted the edited *lep-5* alignment into a hidden Markov model (HMM). Searching other non-*Elegans* supergroup *Caenorhabditis* genomes with the 24-species HMM and *nhmmer* (Wheeler and Eddy, 2013) identified two more *lep-5* loci from *Caenorhabditis* spp. 43 and

31. We also attempted HMM searches of non-*Caenorhabditis* species; although this gave various weak similarities, they were neither statistically significant nor similar to one another. We finally aligned the *lep-5* sequences from all 26 *Caenorhabditis* species with MAFFT and visualized their alignment with Jalview (Figure S3).

Analysis of the secondary structure of the *lep-5* transcript—The processed *lep-5* RNA sequence, including the SL1 trans-spliced leader, along with similar information from *lep-5* orthologs from twenty *Elegans* group *Caenorhabditis* species, was analyzed using TurboFold (Harmanci et al., 2011), part of the RNAstructure package (<http://rna.urmc.rochester.edu/RNAstructure.html>). To model *lep-5*(G23A) and *lep-5*(G23A C30T), corresponding changes were made to all twenty orthologous sequences. The folding temperature was set at 293.15°K (20°C); default parameters were used for all other settings. Structures were drawn using VARNA (Darty et al., 2009). Nucleotide positions were color-coded for confidence level and primary sequence conservation as described in the text. VARNA linear-format representations of Turbofold structures for all species were arranged according to an unpublished phylogenetic tree for *Caenorhabditis* inferred by K. Kiontke using molecular data from 17 loci (RhabditinaDB, rhabditina.org), as shown in Figure S4).

Using an independent method of alignment and structure analysis produced very similar results. Specifically, we used CARNA (ver. 1.3.3, linking LocARNA 1.9.1, Gecode 5.0.0, Vienna RNA package 2.3.2; <http://rna.informatik.uni-freiburg.de>) (Raden et al., 2018; Sorescu et al., 2012) and RNAalifold (<http://rna.tbi.univie.ac.at/cgi-bin/RNAWebSuite/RNAalifold.cgi>). CARNA generated a dot-plot of probabilities of basepairing which was used to generate a consensus sequence and structure, used in an iterative manner to optimize an alignment based on secondary structure conservation. This alignment was very slightly modified by hand to allow a couple additional gaps to further optimize the alignment to the average structure. This alignment was used as input to RNAalifold to generate a consensus RNA structure in which alignment positions were highlighted with regard to conservation and basepair co-variance. Although the resulting structure differed in several details from that shown in Fig. 2A of this paper, there were three regions that were essentially identical: the 5' stem-loop involving SL1, the 3' stem-loop, and the central “zipper” region. Thus, very different structure-alignment methods yield essentially similar results with regard to these three important regions (highlighted red, blue and green, respectively, in Figs. 2 and S4).

Search for miRNA binding sites in the *lep-5* transcript—The *lep-5* sequence was scanned for miRNA binding sites using algorithms available on www.microrna.org, www.targetscan.org and the website of the Segal lab https://genie.weizmann.ac.il/pubs/mir07/mir07_prediction.html (Kertesz et al., 2007). High scoring miRNAs found by all three algorithms are miR-76, miR-265, miR-1830 and miR-2220. None of these miRNAs has been implicated in the heterochronic pathway.

QUANTIFICATION AND STATISTICAL ANALYSIS

For statistical analysis of the RNA co-IP experiments, we used a moderated T-test as described above in the Method Details, “RNA co-IP with LEP-2, LIN-28 and LIN-41” section.

Supplementary Material

Refer to Web version on PubMed Central for supplementary material.

ACKNOWLEDGEMENTS

We thank K. Nguyen for technical help in the screen yielding *ny10* and A. Woronik for help with statistical analyses. We thank V. Ambros, G. Ruvkun, T. Montgomery, D. Mathews, S. Bellaousov, A. Mason, A. Samuelson, L. Maquat, D. Moerman, C. Hammel, S. West and WormBase for constructive discussions and information, F. Slack, V. Ambros, and A. Rougvie for strains, and E. Moss for generously providing the LIN-28 antibody. Some strains were provided by the *Caenorhabditis* Genetics Center (University of Minnesota), which is funded by the NIH Office of Research Infrastructure Programs (P40 OD010440). This research was supported by NIH R01 GM100140, NSF DEB 0922012, NYU RCF 002456, and research funds from NYU Shanghai (D.H.A.F.); and NIH R01 GM108885 and NSF IOS 1353075 (D.S.P.). E.V. was supported by the University of Rochester Medical Scientist Training Program, NIH T32 GM007356, and R.A.H. was supported by the New York Consortium for the Advancement of Postdoctoral Scholars, NIH K12 GM102778.

REFERENCES

- Abbott AL, Alvarez-Saavedra E, Miska EA, Lau NC, Bartel DP, Horvitz HR, and Ambros V (2005). The let-7 MicroRNA family members mir-48, mir-84, and mir-241 function together to regulate developmental timing in *Caenorhabditis elegans*. *Dev Cell* 9, 403–414. [PubMed: 16139228]
- Abreu AP, Dauber A, Macedo DB, Noel SD, Brito VN, Gill JC, Cukier P, Thompson IR, Navarro VM, Gagliardi PC, et al. (2013). Central precocious puberty caused by mutations in the imprinted gene MKRN3. *N Engl J Med* 368, 2467–2475. [PubMed: 23738509]
- Ambros V (1989). A hierarchy of regulatory genes controls a larva-to-adult developmental switch in *C. elegans*. *Cell* 57, 49–57. [PubMed: 2702689]
- Ambros V (2011). MicroRNAs and developmental timing. *Curr Opin Genet Dev* 21, 511–517. [PubMed: 21530229]
- Ambros V, and Horvitz HR (1984). Heterochronic mutants of the nematode *Caenorhabditis elegans*. *Science* 226, 409–416. [PubMed: 6494891]
- Arribere JA, Bell RT, Fu BX, Artiles KL, Hartman PS, and Fire AZ (2014). Efficient marker-free recovery of custom genetic modifications with CRISPR/Cas9 in *Caenorhabditis elegans*. *Genetics* 198, 837–846. [PubMed: 25161212]
- Arumugam TU, Davies E, Morita EH, and Abe S (2007). Sequence, expression and tissue localization of a gene encoding a makorin RING zinc-finger protein in germinating rice (*Oryza sativa* L. ssp. Japonica) seeds. *Plant Physiol Biochem* 45, 767–780. [PubMed: 17870591]
- Blumenthal T (2005). Trans-splicing and operons *WormBook* : the online review of *C. elegans* biology, 1–9.
- Brenner S (1974). The genetics of *Caenorhabditis elegans*. *Genetics* 77, 71–94. [PubMed: 4366476]
- Bussing I, Yang JS, Lai EC, and Grosshans H (2010). The nuclear export receptor XPO-1 supports primary miRNA processing in *C. elegans* and *Drosophila*. *EMBO J* 29, 1830–1839. [PubMed: 20436454]
- Camacho C, Coulouris G, Avagyan V, Ma N, Papadopoulos J, Bealer K, and Madden TL (2009). BLAST+: architecture and applications. *BMC Bioinf* 10, 421.
- Cassar PA, Carpenedo RL, Samavarchi-Tehrani P, Olsen JB, Park CJ, Chang WY, Chen Z, Choey C, Delaney S, Guo H et al. (2015). Integrative genomics positions MKRN1 as a novel ribonucleoprotein within the embryonic stem cell gene regulatory network. *EMBO Rep* 16, 1334–1357. [PubMed: 26265008]
- Caygill EE, and Johnston LA (2008). Temporal regulation of metamorphic processes in *Drosophila* by the let-7 and miR-125 heterochronic microRNAs. *Curr Biol* 18, 943–950. [PubMed: 18571409]
- Cech TR, and Steitz JA (2014). The noncoding RNA revolution—trashing old rules to forge new ones. *Cell* 157, 77–94. [PubMed: 24679528]

- Copley MR, Babovic S, Benz C, Knapp DJ, Beer PA, Kent DG, Wohrer S, Treloar DQ, Day C, Rowe K, et al. (2013). The Lin28b-let-7-Hmga2 axis determines the higher self-renewal potential of fetal haematopoietic stem cells. *Nat Cell Biol* 15, 916–925. [PubMed: 23811688]
- Darty K, Denise A, and Ponty Y (2009). VARNA: Interactive drawing and editing of the RNA secondary structure. *Bioinformatics* 25, 1974–1975. [PubMed: 19398448]
- Del Rio-Albrechtsen T, Kiontke K, Chiou S-Y, and Fitch DH (2006). Novel gain-of-function alleles demonstrate a role for the heterochronic gene *lin-41* in *C. elegans* male tail tip morphogenesis. *Dev Biol* 297, 74–86. [PubMed: 16806150]
- Delas MJ, and Hannon GJ (2017). lncRNAs in development and disease: from functions to mechanisms. *Open Biol* 7.
- Diederichs S (2014). The four dimensions of noncoding RNA conservation. *Trends Genet* 30, 121–123. [PubMed: 24613441]
- Ding L, Spencer A, Morita K, and Han M (2005). The developmental timing regulator AIN-1 interacts with miRISCs and may target the argonaute protein ALG-1 to cytoplasmic P bodies in *elegans*. *Mol Cell* 19, 437–447. [PubMed: 16109369]
- Doench JG, Hartenian E, Graham DB, Tothova Z, Hegde M, Smith I, Sullender M, Ebert BL, Xavier RJ, and Root DE (2014). Rational design of highly active sgRNAs for CRISPR-Cas9-mediated gene inactivation. *Nat Biotechnol* 32, 1262–1267. [PubMed: 25184501]
- Eddy SR (2011). Accelerated Profile HMM Searches. *PLoS Comput Biol* 7, e1002195. [PubMed: 22039361]
- Essers PB, Nonnekens J, Goos YJ, Betist MC, Viester MD, Mossink B, Lansu N, Korswagen HC, Jelier R, Brenkman AB, et al. (2015). A Long Noncoding RNA on the Ribosome Is Required for Lifespan Extension. *Cell Rep*.
- Fatica A, and Bozzoni I (2014). Long non-coding RNAs: new players in cell differentiation and development. *Nat Rev Genet* 15, 7–21. [PubMed: 24296535]
- Faunes F, Gundermann DG, Munoz R, Bruno R, and Larrain J (2017). The heterochronic gene *Lin28* regulates amphibian metamorphosis through disturbance of thyroid hormone function. *Dev Biol* 425, 142–151. [PubMed: 28359807]
- Faunes F, and Larrain J (2016). Conservation in the involvement of heterochronic genes and hormones during developmental transitions. *Dev Biol* 416, 3–17. [PubMed: 27297887]
- Flynn RA, and Chang HY (2014). Long noncoding RNAs in cell-fate programming and reprogramming. *Cell Stem Cell* 14, 752–761. [PubMed: 24905165]
- Gao Y, Zhang Z, Li K, Gong L, Yang Q, Huang X, Hong C, Ding M, and Yang H (2017). Linc-DYNC2H1-4 promotes EMT and CSC phenotypes by acting as a sponge of miR-145 in pancreatic cancer cells. *Cell Death Dis* 8, e2924. [PubMed: 28703793]
- Geisler S, and Collier J (2013). RNA in unexpected places: long non-coding RNA functions in diverse cellular contexts. *Nat Rev Mol Cell Biol* 14, 699–712. [PubMed: 24105322]
- Gerstein MB, Lu ZJ, Van Nostrand EL, Cheng C, Arshinoff BI, Liu T, Yip KY, Robilotto R, Rechtsteiner A, Ikegami K, et al. (2010). Integrative analysis of the *Caenorhabditis elegans* genome by the modENCODE project. *Science* 330, 1775–1787. [PubMed: 21177976]
- Gould SJ (1977). *Ontogeny and phylogeny* (Cambridge, Mass: Belknap Press of Harvard University Press).
- Gray TA, Hernandez L, Carey AH, Schaldach MA, Smithwick MJ, Rus K, Marshall Graves JA, Stewart CL, and Nicholls RD (2000). The ancient source of a distinct gene family encoding proteins featuring RING and C(3)H zinc-finger motifs with abundant expression in developing brain and nervous system. *Genomics* 66, 76–86. [PubMed: 10843807]
- Grosswendt S, Filipchuk A, Manzano M, Klironomos F, Schilling M, Herzog M, Gottwein E, and Rajewsky N (2014). Unambiguous identification of miRNA: target site interactions by different types of ligation reactions. *Mol Cell* 54, 1042–1054. [PubMed: 24857550]
- Haeussler M, Schonig K, Eckert H, Eschstruth A, Mianne J, Renaud JB, Schneider-Maunoury S, Shkumatava A, Teboul L, Kent J, et al. (2016). Evaluation of off-target and on-target scoring algorithms and integration into the guide RNA selection tool CRISPOR. *Genome Biol* 17, 148. [PubMed: 27380939]

- Harmanci AO, Sharma G, and Mathews DH (2011). TurboFold: iterative probabilistic estimation of secondary structures for multiple RNA sequences. *BMC Bioinf* 12, 108.
- He F, Song Z, Chen H, Chen Z, Yang P, Li W, Yang Z, Zhang T, Wang F, Wei J, et al. (2018). Long noncoding RNA PVT1–214 promotes proliferation and invasion of colorectal cancer by stabilizing Lin28 and interacting with miR-128. *Oncogene*.
- Hellwig S, and Bass BL (2008). A starvation-induced noncoding RNA modulates expression of Dicer-regulated genes. *Proc Natl Acad Sci U S A* 105, 12897–12902. [PubMed: 18723671]
- Herrera RA, Kiontke K, and Fitch DH (2016). Makorin ortholog LEP-2 regulates LIN-28 stability to promote the juvenile-to-adult transition in *Caenorhabditis elegans*. *Development* 143, 799–809. [PubMed: 26811380]
- Hochbaum D, Zhang Y, Stuckenholtz C, Labhart P, Alexiadis V, Martin R, Knolker HJ, and Fisher AL (2011). DAF-12 regulates a connected network of genes to ensure robust developmental decisions. *PLoS Genet* 7, e1002179. [PubMed: 21814518]
- Hoogewijs D, Houthoofd K, Matthijssens F, Vandesompele J, and Vanfleteren JR (2008). Selection and validation of a set of reliable reference genes for quantitative sod gene expression analysis in *C. elegans*. *BMC Mol Biol* 9, 9. [PubMed: 18211699]
- Huang X, Zhang H, and Zhang H (2011). The zinc-finger protein SEA-2 regulates larval developmental timing and adult lifespan in *C. elegans*. *Development* 138, 2059–2068. [PubMed: 21471153]
- Ji N, and van Oudenaarden A (2012). Single molecule fluorescent in situ hybridization (smFISH) of *C. elegans* worms and embryos *WormBook* : the online review of *C. elegans* biology, 1–16.
- Kato M, de Lencastre A, Pincus Z, and Slack FJ (2009). Dynamic expression of small noncoding RNAs, including novel microRNAs and piRNAs/21U-RNAs, during *Caenorhabditis elegans* development. *Genome Biol* 10, R54. [PubMed: 19460142]
- Katoh K, and Standley DM (2013). MAFFT multiple sequence alignment software version 7: improvements in performance and usability. *Mol Biol Evol* 30, 772–780. [PubMed: 23329690]
- Kertesz M, Iovino N, Unnerstall U, Gaul U, and Segal E (2007). The role of site accessibility in microRNA target recognition. *Nat Genet* 39, 1278–1284. [PubMed: 17893677]
- Kim JH, Park SM, Kang MR, Oh SY, Lee TH, Muller MT, and Chung IK (2005). Ubiquitin ligase MKRN1 modulates telomere length homeostasis through a proteolysis of hTERT. *Genes Dev* 19, 776–781. [PubMed: 15805468]
- Kiontke KC, Felix MA, Ailion M, Rockman MV, Braendle C, Penigault JB, and Fitch DH (2011). A phylogeny and molecular barcodes for *Caenorhabditis*, with numerous new species from rotting fruits. *BMC Evol Biol* 11, 339. [PubMed: 22103856]
- Kopp F, and Mendell JT (2018). Functional Classification and Experimental Dissection of Long Noncoding RNAs. *Cell* 172, 393–407. [PubMed: 29373828]
- Koppen M, Simske JS, Sims PA, Firestein BL, Hall DH, Radice AD, Rongo C, and Hardin JD (2001). Cooperative regulation of AJM-1 controls junctional integrity in *Caenorhabditis elegans* epithelia. *Nat Cell Biol* 3, 983–991. [PubMed: 11715019]
- Kretz M, Siprashvili Z, Chu C, Webster DE, Zehnder A, Qu K, Lee CS, Flockhart RJ, Groff AF, Chow J, et al. (2013). Control of somatic tissue differentiation by the long noncoding RNA TINCR. *Nature* 493, 231–235. [PubMed: 23201690]
- Labun K, Montague TG, Gagnon JA, Thyme SB, and Valen E (2016). CHOPCHOP v2: a web tool for the next generation of CRISPR genome engineering. *Nucleic Acids Res* 44, W272–276. [PubMed: 27185894]
- Lee EW, Kim JH, Ahn YH, Seo J, Ko A, Jeong M, Kim SJ, Ro JY, Park KM, Lee HW, et al. (2012). Ubiquitination and degradation of the FADD adaptor protein regulate death receptor-mediated apoptosis and necroptosis. *Nat Commun* 3, 978. [PubMed: 22864571]
- Lee EW, Lee MS, Camus S, Ghim J, Yang MR, Oh W, Ha NC, Lane DP, and Song J (2009). Differential regulation of p53 and p21 by MKRN1 E3 ligase controls cell cycle arrest and apoptosis. *EMBO J* 28, 2100–2113. [PubMed: 19536131]
- Lee RC, Feinbaum RL, and Ambros V (1993). The *C. elegans* heterochronic gene *lin-4* encodes small RNAs with antisense complementarity to *lin-14*. *Cell* 75, 843–854. [PubMed: 8252621]

- Li MA, Amaral PP, Cheung P, Bergmann JH, Kinoshita M, Kalkan T, Ralser M, Robson S, von Meyenn F, Paramor M, et al. (2017). A lncRNA fine tunes the dynamics of a cell state transition involving *Lin28*, *let-7* and de novo DNA methylation. *Elife* 6, .
- Liu H, Kong X, and Chen F (2017a). Mkrn3 functions as a novel ubiquitin E3 ligase to inhibit Nptx1 during puberty initiation. *Oncotarget* 8, 85102–85109. [PubMed: 29156706]
- Liu W, Yu E, Chen S, Ma X, Lu Y, and Liu X (2017b). Spatiotemporal expression profiling of long intervening noncoding RNAs in *Caenorhabditis elegans*. *Sci Rep* 7, 5195. [PubMed: 28701691]
- Liu Z, and Ambros V (1991). Alternative temporal control systems for hypodermal cell differentiation in *Caenorhabditis elegans*. *Nature* 350, 162–165. [PubMed: 26502479]
- Mason D, Rabinowitz J, and Portman D (2008). *dmd-3*, a doublesex-related gene regulated by *tra-1*, governs sex-specific morphogenesis in *C. elegans*. *Development* 135, 2373–2382. [PubMed: 18550714]
- Montague TG, Cruz JM, Gagnon JA, Church GM, and Valen E (2014). CHOPCHOP: a CRISPR/Cas9 and TALEN web tool for genome editing. *Nucleic Acids Res* 42, W401–407. [PubMed: 24861617]
- Morita K, and Han M (2006). Multiple mechanisms are involved in regulating the expression of the developmental timing regulator *lin-28* in *Caenorhabditis elegans*. *EMBO J* 25, 5794–5804. [PubMed: 17139256]
- Mortazavi A, Schwarz EM, Williams B, Schaeffer L, Antoshechkin I, Wold BJ, and Sternberg PW (2010). Scaffolding a *Caenorhabditis* nematode genome with RNA-seq. *Genome Res* 20, 1740–1747. [PubMed: 20980554]
- Moss EG, Lee RC, and Ambros V (1997). The cold shock domain protein LIN-28 controls developmental timing in *C. elegans* and is regulated by the *lin-4* RNA. *Cell* 88, 637–646. [PubMed: 9054503]
- Nam JW, and Bartel DP (2012). Long noncoding RNAs in *C. elegans*. *Genome Res* 22, 25292540.
- Nelson MD, and Fitch DH (2011). Overlap extension PCR: an efficient method for transgene construction. *Methods Mol Biol* 772, 459–470. [PubMed: 22065455]
- Nelson MD, Zhou E, Kiontke K, Fradin H, Maldonado G, Martin D, Shah K, and Fitch DH (2011). A bow-tie genetic architecture for morphogenesis suggested by a genome-wide RNAi screen in *Caenorhabditis elegans*. *PLoS Genet* 7, e1002010. [PubMed: 21408209]
- Nguyen CQ, Hall DH, Yang Y, and Fitch DH (1999). Morphogenesis of the *Caenorhabditis elegans* male tail tip. *Dev Biol* 207, 86–106. [PubMed: 10049567]
- Ong KK, Elks CE, Li S, Zhao JH, Luan J, Andersen LB, Bingham SA, Brage S, Smith GD, Ekelund U et al. (2009). Genetic variation in LIN28B is associated with the timing of puberty. *Nat Genet* 41, 729–733. [PubMed: 19448623]
- Paix A, Folkmann A, Rasoloson D, and Seydoux G (2015). High Efficiency, Homology-Directed Genome Editing in *Caenorhabditis elegans* Using CRISPR-Cas9 Ribonucleoprotein Complexes. *Genetics* 201, 47–54. [PubMed: 26187122]
- Peng F, Li TT, Wang KL, Xiao GQ, Wang JH, Zhao HD, Kang ZJ, Fan WJ, Zhu LL, Li M, et al. (2017). H19/*let-7*/LIN28 reciprocal negative regulatory circuit promotes breast cancer stem cell maintenance. *Cell Death Dis* 8, e2569. [PubMed: 28102845]
- Pepper AS, Killian DJ, and Hubbard EJ (2003). Genetic analysis of *Caenorhabditis elegans glp-1* mutants suggests receptor interaction or competition. *Genetics* 163, 115–132. [PubMed: 12586701]
- Perry JR, Stolk L, Franceschini N, Lunetta KL, Zhai G, McArdle PF, Smith AV, Aspelund T, Bandinelli S, Boerwinkle E, et al. (2009). Meta-analysis of genome-wide association data identifies two loci influencing age at menarche. *Nat Genet* 41, 648–650. [PubMed: 19448620]
- Pfaffl MW (2001). A new mathematical model for relative quantification in real-time RT-PCR. *Nucleic Acids Res* 29, e45. [PubMed: 11328886]
- Quinn JJ, and Chang HY (2016). Unique features of long non-coding RNA biogenesis and function. *Nat Rev Genet* 17, 47–62. [PubMed: 26666209]
- Raden M, Ali SM, Alkhnabashi OS, Busch A, Costa F, Davis JA, Eggenhofer F, Gelhausen R, Georg J, Heyne S, et al. (2018). Freiburg RNA tools: a central online resource for RNA-focused research and teaching. *Nucleic Acids Res* 46, W25–W29. [PubMed: 29788132]

- Ransohoff JD, Wei Y, and Khavari PA (2018). The functions and unique features of long intergenic non-coding RNA. *Nat Rev Mol Cell Biol* 19, 143–157. [PubMed: 29138516]
- Reinhart BJ, Slack FJ, Basson M, Pasquinelli AE, Bettinger JC, Rougvie AE, Horvitz HR, and Ruvkun G (2000). The 21-nucleotide *let-7* RNA regulates developmental timing in *Caenorhabditis elegans*. *Nature* 403, 901–906. [PubMed: 10706289]
- Ritchie ME, Phipson B, Wu D, Hu Y, Law CW, Shi W, and Smyth GK (2015). limma powers differential expression analyses for RNA-sequencing and microarray studies. *Nucleic Acids Res* 43, e47. [PubMed: 25605792]
- Rougvie AE, and Moss EG (2013). Developmental transitions in *C. elegans* larval stages. *Curr Top Dev Biol* 105, 153–180. [PubMed: 23962842]
- Rybak-Wolf A, Jens M, Murakawa Y, Herzog M, Landthaler M, and Rajewsky N (2014). A variety of dicer substrates in human and *C. elegans*. *Cell* 159, 1153–1167. [PubMed: 25416952]
- Salvatico J, Kim JH, Chung IK, and Muller MT (2010). Differentiation linked regulation of telomerase activity by Makorin-1. *Mol Cell Biochem* 342, 241–250. [PubMed: 20473778]
- Seggerson K, Tang L, and Moss EG (2002). Two genetic circuits repress the *Caenorhabditis elegans* heterochronic gene *lin-28* after translation initiation. *Dev Biol* 243, 215–225. [PubMed: 11884032]
- Shyh-Chang N, and Daley GQ (2013). Lin28: primal regulator of growth and metabolism in stem cells. *Cell Stem Cell* 12, 395–406. [PubMed: 23561442]
- Sokol NS, Xu P, Jan YN, and Ambros V (2008). *Drosophila* let-7 microRNA is required for remodeling of the neuromusculature during metamorphosis. *Genes Dev* 22, 1591–1596. [PubMed: 18559475]
- Sorescu DA, Mohl M, Mann M, Backofen R, and Will S (2012). CARNA--alignment of RNA structure ensembles. *Nucleic Acids Res* 40, W49–53. [PubMed: 22689637]
- Stefani G, Chen X, Zhao H, and Slack FJ (2015). A novel mechanism of LIN-28 regulation of *let-7* microRNA expression revealed by in vivo HITS-CLIP in *C. elegans*. *RNA* 21, 985–996. [PubMed: 25805859]
- Sulston JE, Albertson DG, and Thomson JN (1980). The *Caenorhabditis elegans* male: postembryonic development of nongonadal structures. *Dev Biol* 78, 542–576. [PubMed: 7409314]
- Thornton JE, and Gregory RI (2012). How does Lin28 let-7 control development and disease? *Trends Cell Biol* 22, 474–482. [PubMed: 22784697]
- Tsialikas J, Romens MA, Abbott A, and Moss EG (2017). Stage-Specific Timing of the microRNA Regulation of lin-28 by the Heterochronic Gene lin-14 in *Caenorhabditis elegans*. *Genetics* 205, 251–262. [PubMed: 27815363]
- Tsialikas J, and Romer-Seibert J (2015). LIN28: roles and regulation in development and beyond. *Development* 142, 2397–2404. [PubMed: 26199409]
- Vadla B, Kemper K, Alaimo J, Heine C, and Moss EG (2012). *lin-28* controls the succession of cell fate choices via two distinct activities. *PLoS Genet* 8, e1002588. [PubMed: 22457637]
- Van Wynsberghe PM, Kai ZS, Massirer KB, Burton VH, Yeo GW, and Pasquinelli AE (2011). LIN-28 co-transcriptionally binds primary *let-7* to regulate miRNA maturation in *Caenorhabditis elegans*. *Nat Struct Mol Biol* 18, 302–308. [PubMed: 21297634]
- Wang KC, and Chang HY (2011). Molecular mechanisms of long noncoding RNAs. *Mol Cell* 43, 904–914. [PubMed: 21925379]
- Wang W, Zhu Y, Li S, Chen X, Jiang G, Shen Z, Qiao Y, Wang L, Zheng P, and Zhang Y (2016). Long noncoding RNA MALAT1 promotes malignant development of esophageal squamous cell carcinoma by targeting beta-catenin via Ezh2. *Oncotarget* 7, 25668–25682. [PubMed: 27015363]
- Waterhouse AM, Procter JB, Martin DM, Clamp M, and Barton GJ (2009). Jalview Version 2--a multiple sequence alignment editor and analysis workbench. *Bioinformatics* 25, 1189–1191. [PubMed: 19151095]
- Weaver BP, Weaver YM, Mitani S, and Han M (2017). Coupled Caspase and N-End Rule Ligase Activities Allow Recognition and Degradation of Pluripotency Factor LIN-28 during Non-Apoptotic Development. *Dev Cell* 41, 665–673 e666. [PubMed: 28602583]
- Weaver BP, Zabinsky R, Weaver YM, Lee ES, Xue D, and Han M (2014). CED-3 caspase acts with miRNAs to regulate non-apoptotic gene expression dynamics for robust development in *C. elegans*. *Elife* 3, e04265. [PubMed: 25432023]

- Wei S, Chen H, Dzakah EE, Yu B, Wang X, Fu T, Li J, Liu L, Fang S, Liu W, et al. (2019). Systematic evaluation of *C. elegans* lincRNAs with CRISPR knockout mutants. *Genome Biol* 20, 7. [PubMed: 30621757]
- Wheeler TJ, and Eddy SR (2013). nhmmer: DNA homology search with profile HMMs. *Bioinformatics* 29, 2487–2489. [PubMed: 23842809]
- Wightman B, Ha I, and Ruvkun G (1993). Posttranscriptional regulation of the heterochronic gene *lin-14* by *lin-4* mediates temporal pattern formation in *C. elegans*. *Cell* 75, 855–862. [PubMed: 8252622]
- Wu YC, Chen CH, Mercer A, and Sokol NS (2012). let-7-complex microRNAs regulate the temporal identity of *Drosophila* mushroom body neurons via chinmo. *Dev Cell* 23, 202–209. [PubMed: 22814608]
- Yoon JH, Abdelmohsen K, Kim J, Yang X, Martindale JL, Tominaga-Yamanaka K, White EJ, Orjalo AV, Rinn JL, Kreft SG, et al. (2013). Scaffold function of long non-coding RNA HOTAIR in protein ubiquitination. *Nat Commun* 4, 2939. [PubMed: 24326307]
- Zhang J, Ratanasirintrao S, Chandrasekaran S, Wu Z, Ficarro SB, Yu C, Ross CA, Cacchiarelli D, Xia Q, Seligson M, et al. (2016). LIN28 Regulates Stem Cell Metabolism and Conversion to Primed Pluripotency. *Cell Stem Cell* 19, 66–80. [PubMed: 27320042]
- Zhu H, Shah S, Shyh-Chang N, Shinoda G, Einhorn WS, Viswanathan SR, Takeuchi A, Grasmann C, Rinn JL, Lopez MF, et al. (2010). Lin28a transgenic mice manifest size and puberty phenotypes identified in human genetic association studies. *Nat Genet* 42, 626–630. [PubMed: 20512147]
- Zisoulis DG, Lovci MT, Wilbert ML, Hutt KR, Liang TY, Pasquinelli AE, and Yeo GW (2010). Comprehensive discovery of endogenous Argonaute binding sites in *Caenorhabditis elegans*. *Nat Struct Mol Biol* 17, 173–179. [PubMed: 20062054]

HIGHLIGHTS

- *lep-5* acts in the heterochronic pathway to promote the larval-to-adult transition
- *lep-5* is a ~600-nt, highly structured lncRNA that is conserved across *Caenorhabditis*
- Like the Makorin LEP-2, *lep-5* promotes the degradation of LIN-28 protein
- *lep-5* may act as a scaffold to bring LEP-2 into close proximity with LIN-28

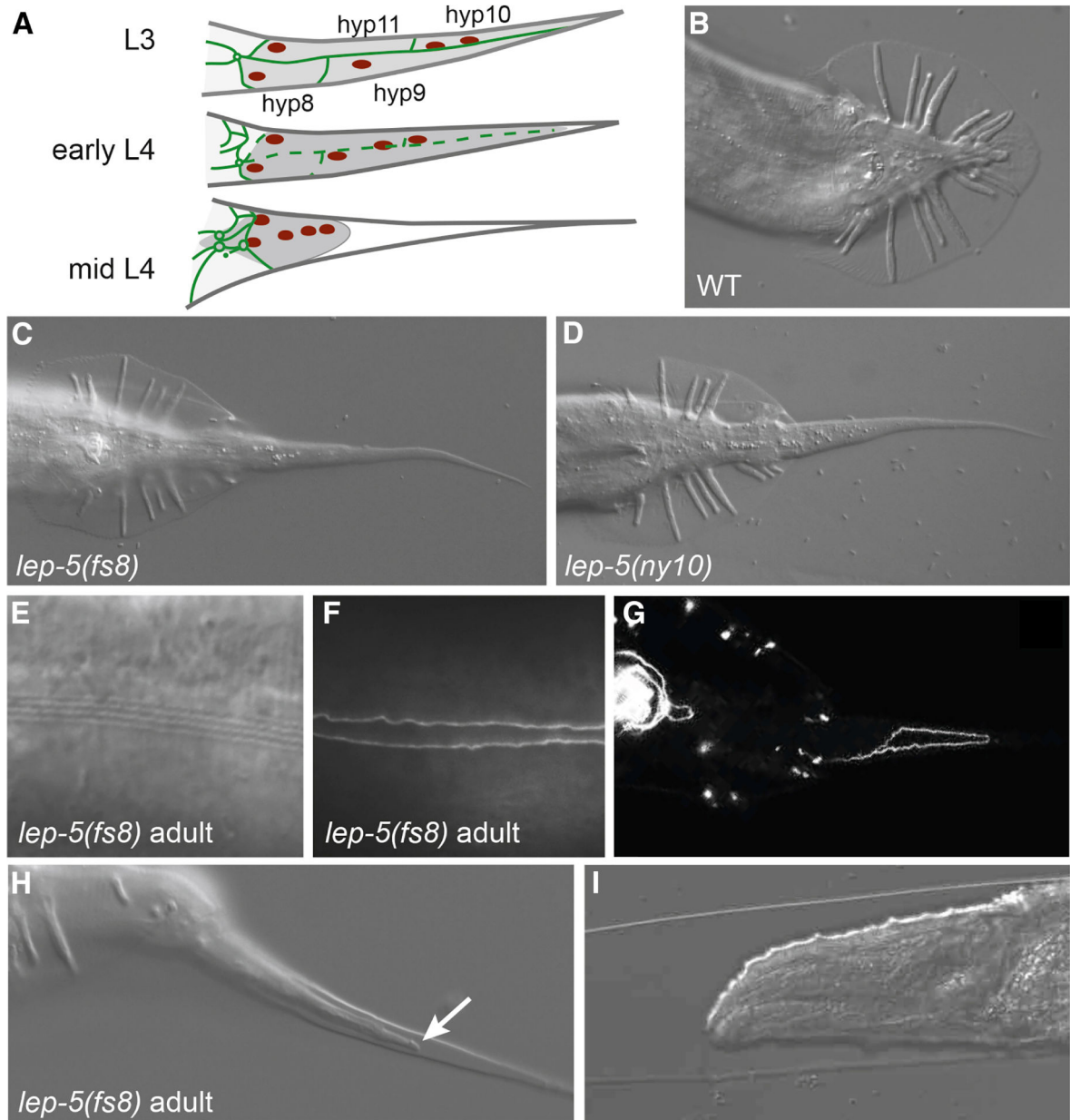


Figure 1. *lep-5* is required for male tail tip morphogenesis.

(A) Schematic of TTM in lateral view. Tail tip cytoplasm shaded dark grey, adherens junctions green, nuclei red. The L3 tail tip is long and pointed. In early L4, TTM begins with fusion of the four tail tip cells (adherens junctions degrade) and retraction away from the cuticle in the posterior. By mid-L4, the tail tip syncytium has rounded and is migrating anteriorly. (B-D) Adult tails of WT, *lep-5(fs8)* and *lep-5(ny10)* mutant males in ventral view. (E) DIC image of normal alae in a *lep-5(fs8)* adult male. (F) *ajm-1::GFP* labeling of adherens junctions shows fully fused lateral seam in a *lep-5(fs8)* adult male. (G) Incompletely fused tail tip cells in an adult *lep-5(fs8)* male display persisting *ajm-1::GFP*. (H) Adult TTM in a *lep-5(fs8)* male; arrow points to retracting tissue under the adult cuticle;

lateral view. (I) Anterior end of a *lep-5* adult trapped inside the cuticle from a supernumerary molt. See also Figure S1.

Author Manuscript

Author Manuscript

Author Manuscript

Author Manuscript

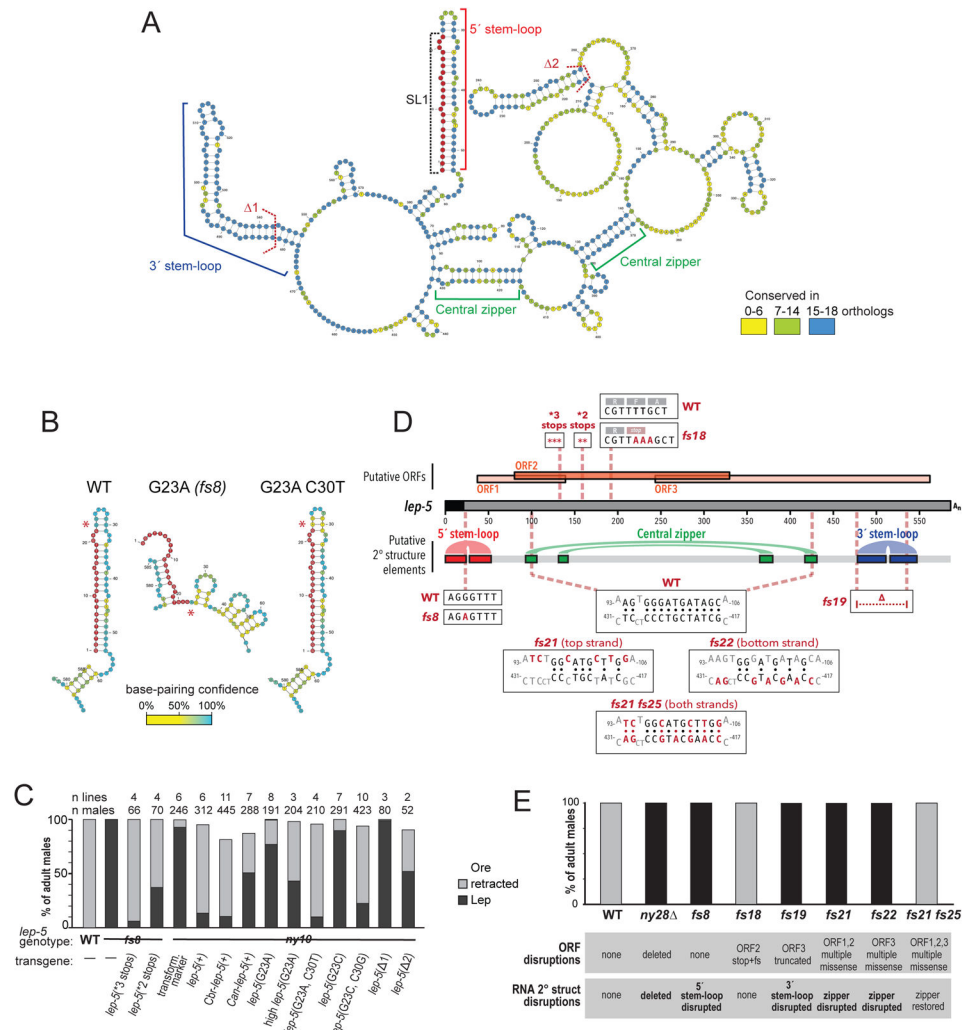


Figure 2. *lep-5* is a long non-coding RNA.

(A) The secondary structure of the *lep-5* lncRNA as predicted by Turbofold. The conserved 5' stem-loop (red bracket) includes the SL1 trans-spliced leader (in red). The 3' stem-loop (blue bracket) and two base-paired regions forming the “central zipper” (green brackets) are also conserved. Dashed lines: boundaries of two hairpins deleted in the rescue experiments (1 and 2). The polyA tail is omitted for clarity. For alignments, see Fig. S3 and STAR Methods. The 5' region from predicted full-length structures of wild-type *lep-5*, *lep-5(fs8 = G23A)* and *lep-5(G23A, C30T)*. Asterisks indicate position 23. SL1 is in red. See also Figures S4, S5. (C) Rescue experiments with transgenes containing stop codons in the predicted coding region (*3 or *2 stops), the *lep-5* orthologs of *C. briggsae* and *C. angaria* and constructs containing nucleotide substitutions that disrupt and restore the *lep-5* secondary structure (high *lep-5(G23A)* = transgene at 10x concentration). (D) Schematic of the SL1-spliced *lep-5* RNA with putative ORFs shown above and selected predicted secondary structure features shown below. Boxes show the sequence of various mutant alleles compared with the wild-type allele. (E) Male tail tip phenotype at 20°C of *lep-5* mutants in which the secondary structure and/or the predicted ORFs are disrupted.

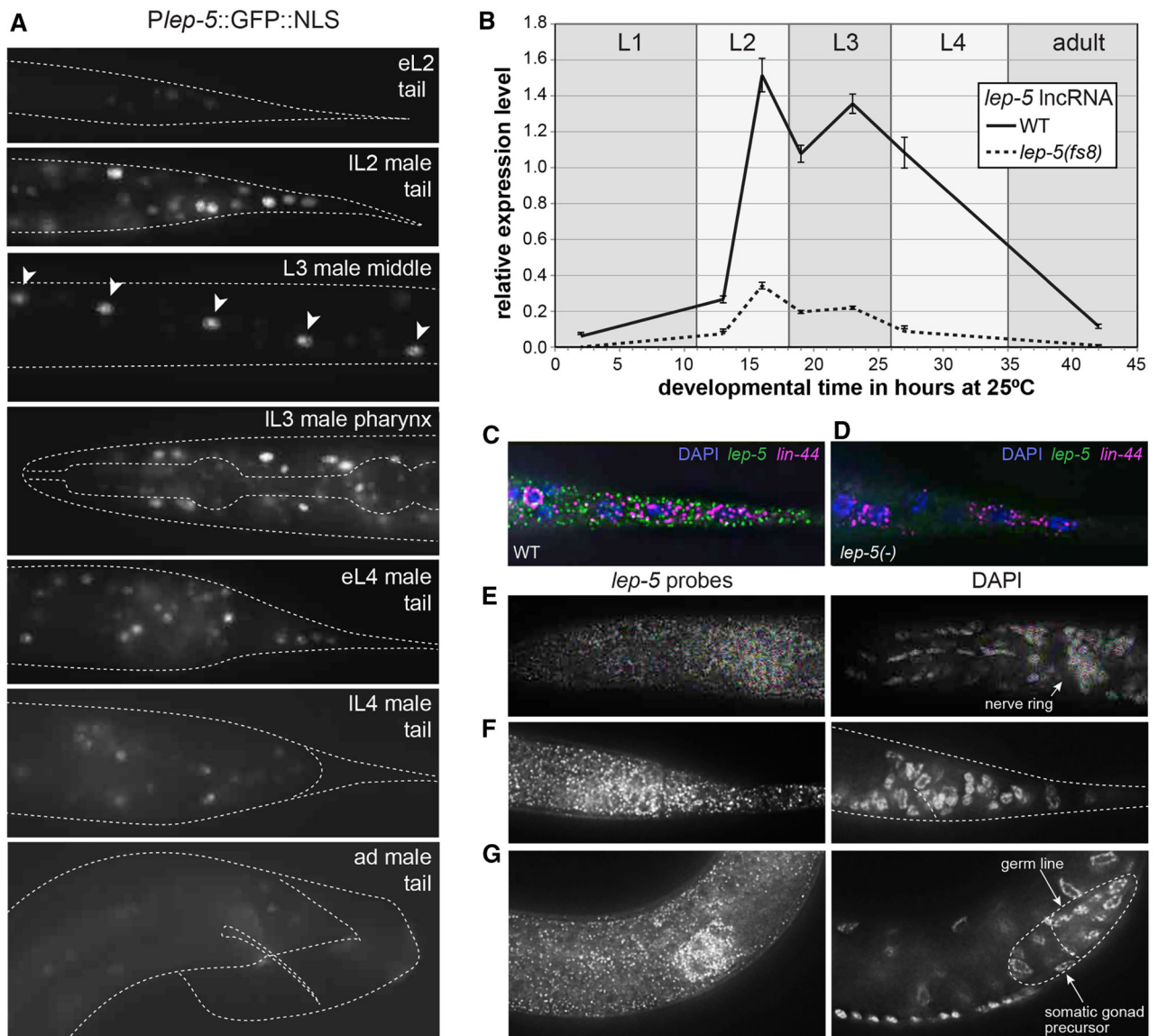


Figure 3. *lep-5* lncRNA expression is temporally regulated.

(A) Temporal expression of *Plep-5::GFP::NLS* in late L1 animals (top) through adults (bottom). Expression is observed in the tail epidermis including the tail tip cells, in pharynx muscles, in neurons in the head and cloacal region, and in seam cells (arrowheads). (B) Temporal expression of *lep-5* lncRNA from L1 to adult as measured by qPCR. Error bars show SD. (C, D) *lep-5* lncRNA visualized with smFISH probes in the tail tip of a wild-type and *lep-5(ny10)* L2 animal. *lin-44* probes were used as positive control. DAPI staining indicates nuclei. (E-G) Late L2 male. *lep-5* lncRNA visualized with smFISH probes (left) and nuclei stained with DAPI (right) showing areas of concentrated *lep-5* lncRNA expression in the ganglia in the pharynx (E) and rectal (F) region and in the somatic portion of the developing gonad (G). See also Figure S6.

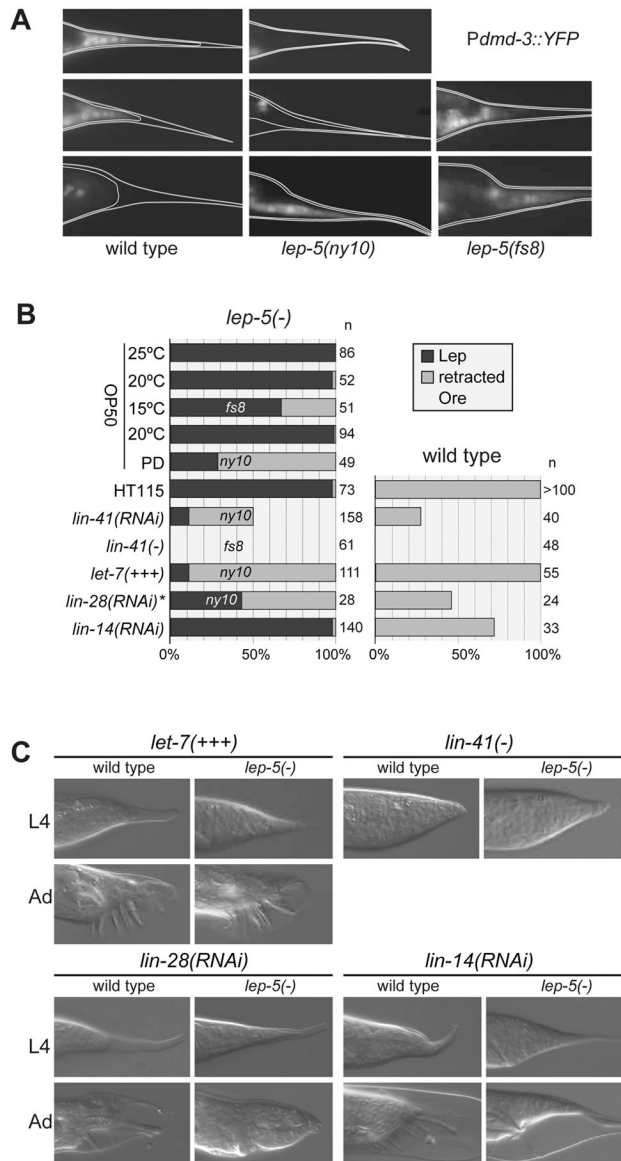


Figure 4. *lep-5* functions upstream of *lin-28* in the heterochronic pathway to control TTM.

(A) Expression of *Pdm-3::YFP* in wild-type and mutant male tail tips at early (e), mid (m) and late (l) L4 stage. (B) Penetrance and expressivity of tail tip phenotypes in single mutants, double mutants and mutant/RNAi knockdown combinations. Left column shows results in a *lep-5* mutant background (relevant allele indicated); right column shows corresponding result in a wild-type background. PD = post dauer, HT115 = RNAi control bacterial strain, asterisk: RNAi fed to L1 larvae. (C) DIC images of representative L4 and adult male tails from the experiments summarized in (B). A rounded tail tip in L4 results from precocious TTM in L3. Adults shown for *lin-14(RNAi)* have just molted and remain surrounded by the L4 cuticle. See also Figure S7.

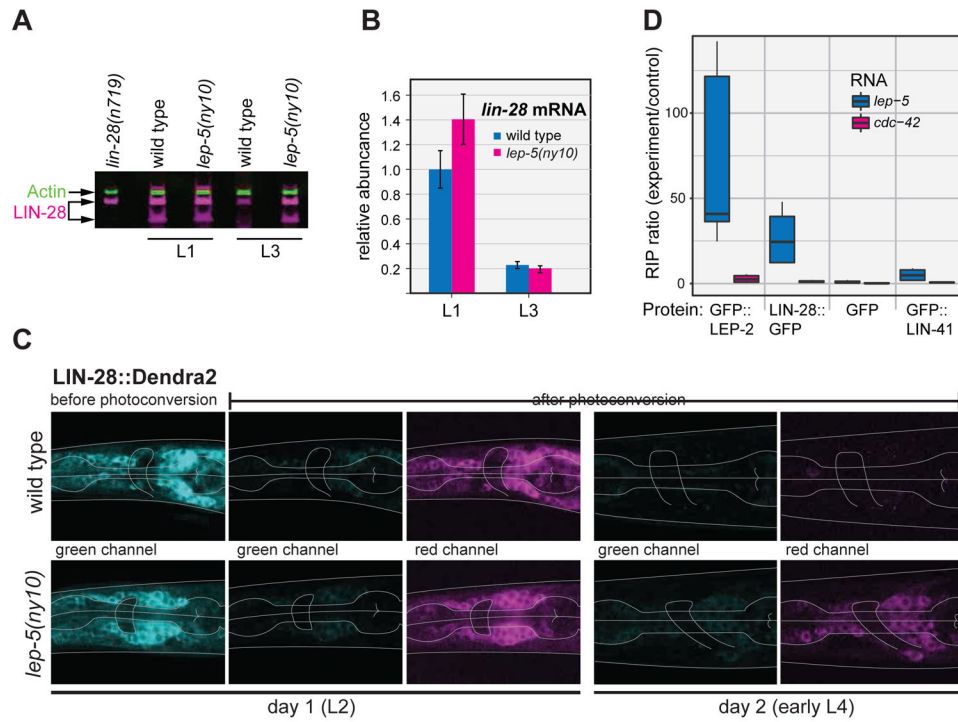
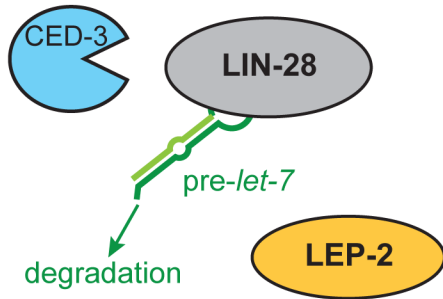


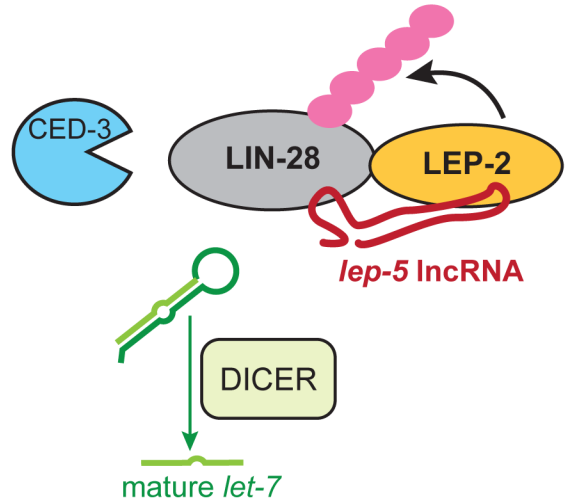
Figure 5. *lep-5* lncRNA promotes LIN-28 degradation.

(A) Detection of endogenous LIN-28 protein by Western blot (actin used for a normalization control). (B) *lin-28* mRNA levels determined by qPCR. Values are normalized to wild-type L1s. (C) Analysis of a LIN-28::Dendra2 fusion protein in WT (top) and *lep-5(ny10)* (bottom) males. Shown are neurons in the head region (pharynx and nerve ring indicated by grey lines). From left to right: green fluorescent signal before photoconversion, diminished green signal after photoconversion, red signal after photoconversion, green and red signals in the same animals 24 hours later. (D) Ratios of *lep-5* lncRNA and control mRNA for *cdc-42* in immune-precipitation of GFP-tagged proteins using anti-GFP relative to negative control IP measured by qPCR (see STAR Methods for details). For each set of triplicate experiments, the first to third quartile is represented as a box, the median as a black bar and the maximum and minimum values as whiskers.

L1: slow LIN-28 degradation



L3: rapid LIN-28 degradation

**Figure 6. Model for *lep-5* function as an instructive switch for LIN-28 degradation.**

(Left) Early during *C. elegans* development, before the onset of *lep-5* expression, slow degradation of LIN-28 is facilitated by CED-3 (Weaver et al., 2014). LEP-2, a putative E3 ligase, is present but does not efficiently ubiquitinate LIN-28. LIN-28 facilitates the degradation of *pre-let-7*. (Right) Later, e.g. in L3, *lep-5* acts as a scaffold to bring LEP-2 and LIN-28 into close proximity, allowing efficient ubiquitination of LIN-28. Ubiquitinated LIN-28 would then be subject to rapid proteasomal degradation. When LIN-28 is absent, *let-7* biogenesis can proceed, leading to adult-specific programs of TTM, production of adult cuticle and exit from the molting cycle.

Table 1.

Tail tip phenotypes of adult males

Genotype	% Lep	% WT	% Ore	<i>n</i>
<i>lep-5(ny10)</i> , 25°C	99	1	0	94
<i>lep-5(fs8)</i> , 25°C	100	0	0	86
<i>lep-5(fs8)</i> , 20°C	98	2	0	52
<i>lep-5(fs8)</i> , 15°C	67	33	0	51
<i>lep-5(ny10)</i> , post-dauer	29	71	0	49
<i>lep-5(ny10)</i> , fed on HT115	97	3	0	73
<i>lep-5(ny28)</i> , 25°C	100	0	0	30
<i>lep-5(ny28)</i> , 20°C	100	0	0	37
<i>lep-5(ny28)</i> , 15°C	98	2	0	46
<i>lep-5(fs18)</i> , 25°C	0	100	0	31
<i>lep-5(fs18)</i> , 20°C	0	100	0	50
<i>lep-5(fs18)</i> , 15°C	0	100	0	47
<i>lep-5(fs19)</i> , 25°C	100	0	0	53
<i>lep-5(fs19)</i> , 20°C	100	0	0	37
<i>lep-5(fs19)</i> , 15°C	100	0	0	43
<i>lep-5(fs21)</i> , 25°C	100	0	0	33
<i>lep-5(fs21)</i> , 20°C	100	0	0	39
<i>lep-5(fs21)</i> , 15°C	98	2	0	50
<i>lep-5(fs22)</i> , 25°C	100	0	0	31
<i>lep-5(fs22)</i> , 20°C	100	0	0	43
<i>lep-5(fs22)</i> , 15°C	100	0	0	43
<i>lep-5(fs21fs25)</i> , 25°C	0	100	0	43
<i>lep-5(fs21fs25)</i> , 20°C	0	100	0	51
<i>lep-5(fs21fs25)</i> , 15°C	0	100	0	43
<i>lin-41(ma104)</i>	0	0	100	61
<i>lin-41(ma104); lep-5(fs8)</i>	0	0	100	48
<i>lin-41(RNAi)</i>	0	28	74	40
<i>lin-41(RNAi); lep-5(ny10)</i>	11	39	50	158
<i>zals3[let-7(+)+myo-3::GFP]^a</i>	0	100	0	55
<i>lep-5(ny10); zals3</i>	2	89	0	111
<i>lin-28(RNAi)</i>	0	46	54	24
<i>lin-28(RNAi); lep-5(ny10)</i>	43	57	0	28
<i>lin-14(RNAi)</i>	0	72	28	32
<i>lin-14(RNAi); lep-5(ny10)</i>	98	2	0	140

^a72% of males begin tail tip retraction during the L3 stage (*n* = 54)

KEY RESOURCES TABLE

REAGENT or RESOURCE	SOURCE	IDENTIFIER
Antibodies		
Mouse Anti-Actin Monoclonal Antibody, Unconjugated, Clone AC-40	Sigma-Aldrich	Sigma-Aldrich Cat# A4700, RRID:AB_476730
Rabbit anti-LIN-28 polyclonal antibody	Eric Moss lab Seggerson et al. 2002	n/a
IRDye 800CW Goat anti-Mouse	LI-COR	LI-COR Biosciences Cat# 827-08364, RRID:AB_10793856
IRDye 680RD Goat anti-Rabbit	LI-COR	LI-COR Biosciences Cat# 926-68171, RRID:AB_10956389
Bacterial and Virus Strains		
OP50-1		RRID:WB-STRAIN:OP50-1
Chemicals, Peptides, and Recombinant Proteins		
Alt-R® S.p. Cas9 Nuclease	Integrated DNA Technologies (IDT)	Cat#1081058
Restriction enzyme SfiI	New England Biolabs	Cat#R0123S
Restriction enzyme AatII	New England Biolabs	Cat#R0117S
Critical Commercial Assays		
QuikChangeXL site-directed mutagenesis kit	Agilent Technologies	Cat#200516
Custom Stellaris RNA-FISH probes for <i>lep-5</i> labeled with Quasar570 (sequences in STAR methods)	Biosearch Technologies	https://www.biosearchtech.com/products/rna-fish
Custom Stellaris RNA-Fish probes for <i>lin-44</i> labeled with Quasar670 (sequences in STAR methods)	Biosearch Technologies	https://www.biosearchtech.com/products/rna-fish
RNeasy micro kit	Qiagen	Cat#74004
double-primed RNA to cDNA EcoDry Premix	Takara/Clontech	Cat #639547
iQ SYBR Green Supermix	BioRad	Cat#1708882
GFP-Trap MA and	Chromotek	Cat#gtma-20
Binding control for GFP-Trap MA	Chromotek	Cat#bmab-20
Experimental Models: Organisms/Strains		
<i>C. elegans</i> CB4088 = <i>him-5(e1490)V</i>	CGC	https://cgc.umn.edu/strain/CB4088
<i>C. elegans</i> DF135 = <i>him-5(e1490) V; lep-5(ny10) X</i>	This paper	n/a
<i>C. elegans</i> DF137 = <i>him-5(e1490) V; lep-5(ny10) X; f5Is2[Pdmd-3::yfp + CC::GFP]</i>	This paper	n/a
<i>C. elegans</i> DF174 = <i>him-5(e1490) V; lep-5(ny10) X; nyEx23[Plin-41::NLS::GFP + rol-6]</i>	This paper	n/a
<i>C. elegans</i> DF213 = <i>him-5(e1490) V; zaIs3[let-7(+)+ myo-3::GFP]</i> made by crossing CT19 with CB4088	This paper	n/a
<i>C. elegans</i> DF223 = <i>him-5(e1490) V; lep-5(ny10)X; zaIs3[let-7(+)+ myo-3::GFP]</i>	This paper	n/a
<i>C. elegans</i> DF235 = <i>him-5(e1490) V; lep-5(ny10) X; wIs78[unc-119(+)+ ajm-1::GFP + scm::GFP + F58E10(+)]</i>	This paper	n/a

REAGENT or RESOURCE	SOURCE	IDENTIFIER
<i>C. elegans</i> DF237 = <i>him-5(e1490) V</i> ; <i>malS108[lin-28::gfp + rol-6]</i>	This paper	n/a
<i>C. elegans</i> DF293 = <i>lep-2(ny23) IV</i> ; <i>him-5(e1490) V</i> ; <i>nyEx53[lep-2>GFP::lep-2b + pRF4]</i>	This paper	n/a
<i>C. elegans</i> DF282 = <i>lin-41(tm1541[GFP::tev::s::lin-41]) I</i> ; <i>him-5(e1490) V</i>	This paper	n/a
<i>C. elegans</i> DF302 = <i>him-5(e1490) V</i> ; <i>nyEx61[lep-5>GFP + rol-6]</i>	This paper	n/a
<i>C. elegans</i> DF271 = <i>him-5(e1490) V</i> ; <i>nyEx56[lin-28::Dendra2::lin-28_3'UTR + rol-6]</i>	Herrera et al. 2016	n/a
<i>C. elegans</i> EM122 = <i>him-5(e1490) V</i> ; <i>unc-18(e81) dpy6(e14) X</i>	CGC	https://cgc.umn.edu/strain/EM122
<i>C. elegans</i> UR290 = <i>him-5(e1490) V</i> ; <i>lep-5(fs8) X</i>	This paper	n/a
<i>C. elegans</i> UR1140 = <i>him-5(e1490) V</i> ; <i>lep-5(fs18) X</i>	This paper	n/a
UR157 = <i>fsIs2[dmd-3promxln2::YFP + CCGFP] I</i> ; <i>him-5(e1490) V</i>	This paper	n/a
<i>C. elegans</i> UR1141 = <i>him-5(e1490) V</i> ; <i>lep-5(fs19) X</i>	This paper	n/a
<i>C. elegans</i> UR1207 = <i>him-5(e1490) V</i> ; <i>lep-5(fs21) X</i>	This paper	n/a
<i>C. elegans</i> UR1208 = <i>him-5(e1490) V</i> ; <i>lep-5(fs22) X</i>	This paper	n/a
<i>C. elegans</i> UR1211 = <i>him-5(e1490) V</i> ; <i>lep-5(fs21 fs25) X</i>	This paper	n/a
<i>C. elegans</i> UR1226 = <i>lin-41(ma104) I</i> ; <i>him-5(e1490) V</i> ; <i>lep-5(fs8) X</i>	This paper	n/a
Oligonucleotides		
See Table S1 for list of oligonucleotides		
Recombinant DNA		
Gateway vector pDONR TM P4-P1R	Life Technologies	Not available (replaced by new product)
RNAi feeding clone for <i>C. elegans</i> lin-14: Ahringer library sjj_T25C12.1	Source BioScience	sjj_T25C12.1
RNAi feeding clone for <i>C. elegans</i> lin-41: Ahringer library sjj_C12C8.3	Source BioScience	sjj_C12C8.3
RNAi feeding clone for <i>C. elegans</i> lin-28: Vidal library GHR-11014@G03	Source BioScience	GHR-11014@G03
L4440 control plasmid for RNAi feeding experiments	Addgene	RRID:Addgene_1654
pRF4[<i>rol-6(d)</i>]		
<i>Punc-122::GFP C. elegans</i> expression vector	Addgene	RRID:Addgene_19325
GFP::NLS <i>C. elegans</i> expression vector	Addgene	RRID:Addgene_1622
<i>Dendra2 C. elegans</i> expression vector	Addgene	RRID:Addgene_40077
Fosmid clones WRM062bG06, WRM0629cE12, WRM0628aE08 and WRM0640cA10	Source BioScience	https://www.sourcebioscience.com/
Software and Algorithms		
imageJ		https://imagej.nih.gov
ChopChop	Labun et al., 2016; Montague et al., 2014	http://chopchop.cbu.uib.no
CRISPOR	Haeussler et al., 2016	http://crispor.tefor.net
ApE	Doench et al., 2014	http://jorgensen.biology.utah.edu/wayned/ape/

REAGENT or RESOURCE	SOURCE	IDENTIFIER
LIMMA		https://bioconductor.org/packages/release/bioc/html/limma.html
HMMER 3.1b2	Eddy, 2011	http://hmmmer.org
MAFFT v7.266	Katoh and Standley, 2013	https://mafft.cbrc.jp/alignment/software/
Jalview 2.9.0b2	Waterhouse et al., 2009	http://www.jalview.org
TurboFold	Harmanci et al., 2011	http://ma.urmc.rochester.edu/RNAstructure.html
VARNA	Darty et al., 2009	http://varna.lri.fr
CARNA	Raden et al., 2018; Sorescu et al., 2012	http://ma.informatik.uni-freiburg.de
RNAalifold		http://ma.tbi.univie.ac.at/cgi-bin/RNAWebSuite/RNAalifold.cgi
TargetScan		http://www.targetscan.org/worm_52/
Online MicroRNA prediction tool	Kertesz et al. 2007	https://genie.weizmann.ac.il/pubs/mir07/mir07_prediction.html
microRNA.org		http://www.microrna.org/microrna/home.do
Other		
Genome sequence of <i>Caenorhabditis afra</i>		http://ensembl.caenorhabditis.org/index.html
Genome sequence of <i>C. brenneri</i>		https://wormbase.org/species/c_brenneri#4--10
Genome sequence of <i>C. briggsae</i>		https://wormbase.org/species/c_briggsae#0--10
Genome sequence of <i>C. doughertyi</i>		http://ensembl.caenorhabditis.org/index.html
Genome sequence of <i>C. japonica</i>		https://wormbase.org/species/c_japonica#0--10
Genome sequence of <i>C. kamaaina</i>		http://ensembl.caenorhabditis.org/index.html
Genome sequence of <i>C. latens</i>		https://parasite.wormbase.org/Caenorhabditis_latens_prjna248912/Info/Index
Genome sequence of <i>C. macrosperma</i>		nematode.org
Genome sequence of <i>C. nigoni</i>		https://parasite.wormbase.org/Caenorhabditis_nigoni_prjna384657/Info/Index
Genome sequence of <i>C. nouraguensis</i>		http://ensembl.caenorhabditis.org/index.html
Genome sequence of <i>C. remanei</i>		https://wormbase.org/species/c_remanei#0--10
Genome sequence of <i>C. sinica</i>		https://parasite.wormbase.org/Caenorhabditis_sinica_prjna194557/Info/Index
Genome sequence of <i>C. sp. 28</i>		http://ensembl.caenorhabditis.org/index.html
Genome sequence of <i>C. sp. 29</i>		http://ensembl.caenorhabditis.org/index.html
Genome sequence of <i>C. sp. 32</i>		http://ensembl.caenorhabditis.org/index.html
Genome sequence of <i>C. sp. 40</i>		http://ensembl.caenorhabditis.org/index.html
Genome sequence of <i>C. tropicalis</i>		https://parasite.wormbase.org/Caenorhabditis_tropicalis_prjna53597/Info/Index
Genome sequence of <i>C. wallacei</i>		nematode.org
Genome sequence of <i>C. angaria</i>		https://wormbase.org/species/all#0123--10
Genome sequence of <i>C. castelli</i>		http://ensembl.caenorhabditis.org/index.html
Genome sequence of <i>C. sp. 38</i>		http://ensembl.caenorhabditis.org/index.html

REAGENT or RESOURCE	SOURCE	IDENTIFIER
Genome sequence of <i>C. pilcata</i>		http://ensembl.caenorhabditis.org/index.html
Genome sequence of <i>C. virilis</i>		http://ensembl.caenorhabditis.org/index.html
Genome sequence of <i>C. sp. 43</i>		http://ensembl.caenorhabditis.org/index.html
Genome sequence of <i>C. sp. 31</i>		http://ensembl.caenorhabditis.org/index.html

Author Manuscript

Author Manuscript

Author Manuscript

Author Manuscript